Publications of the Astronomical Society of the Pacific, 131:016001 (32pp), 2019 January https://doi.org/10.1088/1538-3873/aae856

Radio Stars: From kHz to THz

Lynn D. Matthews
MIT Haystack Observatory, 99 Millstone Road, Westford, MA 01886 USA; lmatthew@haystack.mit.edu
Received 2018 July 20; accepted 2018 October 11; published 2018 December 10

Abstract

Advances in technology and instrumentation have now opened up virtually the entire radio spectrum to the study of stars. An international workshop, "Radio Stars: From kHz to THz", was held at the Massachusetts Institute of Technology Haystack Observatory on 2017 November 1–3 to discuss the progress in solar and stellar astrophysics enabled by radio wavelength observations. Topics covered included the Sun as a radio star; radio emission from hot and cool stars (from the pre- to post-main-sequence); ultracool dwarfs; stellar activity; stellar winds and mass loss; planetary nebulae; cataclysmic variables; classical novae; and the role of radio stars in understanding the Milky Way. This article summarizes meeting highlights along with some contextual background information.

Key words: Sun: general – stars: general – stars: winds – outflows – stars: activity – radio continuum: stars – radio lines: stars – (stars:) circumstellar matter – stars: mass-loss

Online material: color figures

1. Background and Motivation for the Workshop

Detectable radio emission[1] is ubiquitous among stars spanning virtually every temperature, mass, and evolutionary stage. This emission can be either thermal or nonthermal, and may stem from any of several mechanisms, including bremsstrahlung (free–free), gyromagnetic radiation, spectral lines (radio recombination lines (RRLs)), rotational transitions of molecules, and hyperfine atomic transitions), plasma radiation, and the electron cyclotron maser (ECM) mechanism. While radio emission typically comprises only a small fraction of the total stellar luminosity, radio wavelength studies provide insight into a broad range of stellar phenomena that cannot be studied by any other means (Dulk 1985; Hjellming 1988; Linsky 1996; Güdel 2002; Paredes 2005).

Nonthermal stellar radio emission is associated with processes involving shocks or magnetic fields, including magnetospheric activity, stellar pulsations, wind-wind interactions, and jets. The detection of thermal stellar emission is most common from objects with relatively large emitting surfaces (e.g., luminous stars, H II regions, disks, stellar outflows, and ejecta). While the various types of stellar radio emission manifest themselves over several decades in frequency (kHz–THz), they are united by fundamental commonalities in telescope design, detector technologies, and data processing techniques, and they are often complementary in probing the different regions of the atmosphere, wind, and circumstellar environment within a given star or stellar system.

Recent technological advances have led to dramatic improvements in sensitivity and achievable angular, temporal, and spectral resolution for observing stellar radio emission. As a result, stars are now being routinely observed over essentially the entire radio spectrum. To discuss the fruits of these advances, an international workshop, "Radio Stars: from kHz to THz", (hereafter RS-2) was held at the Massachusetts Institute of Technology (MIT) Haystack Observatory in Westford, Massachusetts on 2017 November 1–3. This was a follow-on to the first Haystack Radio Stars workshop (hereafter RS-1) held five years prior (Matthews 2013). RS-2 had 51 registered participants representing 10 countries. A primary motivation was to bring together stellar astrophysicists (including observers, theorists, and modelers) from a variety of subdisciplines to explore common themes in the study of stars across the Hertzsprung-Russell (H-R) diagram, particularly those that exploit the unique potential of the latest generation of radio instruments.

2. Scientific Sessions

The science program of RS-2 comprised oral presentations (12 invited reviews and 24 contributed talks), posters, and a moderated closing discussion session. The complete program and presentation abstracts can be viewed on the meeting website.[2] Slides and audio recordings from many of the presentation are also available at this site.

The workshop was structured around eleven scientific sessions: (I) An Overview of Stellar Radio Astronomy; (II) Radio Emission from Young Stars; (III) Radio Emission

[1] Throughout this article, the term "radio" is used to refer to emission spanning kHz to THz frequencies (i.e., wavelengths from meter to submillimeter).

[2] http://www.haystack.mit.edu/workshop/Radio-Stars2017/

from Hot Stars; (IV) The Sun as a Radio Star; (V) Active Stars; (VI) Cool and Ultracool Dwarfs (UCDs); (VII) Radio Stars as Denizens of the Galaxy; (VIII) Radio Astrophysics across the H-R Diagram; (IX) Radio Emission from Cool, Evolved Stars; (X) Radio Emission beyond the AGB; and (XI) The Future of Stellar Radio Science. In this review, I summarize some highlights from these various sessions, which illustrate the myriad areas of stellar astrophysics that are being advanced by radio observations. My summary is roughly organized around the session topics, although I sometimes deviate from this in an effort to synthesize information from different sessions related to a common theme. I also draw attention to unsolved problems and puzzles that were highlighted at the meeting and where future radio wavelength observations are expected to play a key role in advancing our understanding.

3. An Overview of Stellar Radio Astronomy

A framework for the entire meeting was supplied by the opening presentation of J. Linsky (University of Colorado/National Institute of Standards and Technology). His talk underscored that we are in the midst an exceptionally productive era for stellar radio astrophysics, and he highlighted a wide variety of timely topics, many of which were discussed further by subsequent speakers.

Linsky identified four key areas where stellar radio astronomy has unique potential to advance our understanding of stellar astrophysics: (1) What are the physical processes through which stars control the evolution and habitability of planets? (2) How do young stars and their planets evolve in their common disk environment? (3) How is energy from the stellar magnetic field converted into heat, particle acceleration, and mechanical energy (e.g., mass loss)? (4) What physical processes control mass loss across the H-R diagram, and how does the mass loss affect the different stages of stellar evolution? Linsky also emphasized the growing need for models with predictive power, both at radio wavelengths and across the entire electromagnetic spectrum.

As summarized below, numerous insights into Linsky's key questions were put forward during the workshop. But at the same time—underscoring the vitality of the field—new questions have begun to emerge as the result of better data and modeling.

4. Radio Emission from Pre-main-sequence Stars

4.1. Radio-emission Processes in Young Stars

L. Loinard (Universidad Nacional Autónoma de México) provided an overview of the merits of multi-frequency radio wavelength observations for understanding fundamental physical processes (accretion, ejection, magnetism) in the evolution of low-mass young stellar objects (YSOs), from the protostellar (ages $\sim 10^5$ yr) through the pre-main-sequence (PMS) stages ($\sim 50 \times 10^6$ yr). For YSOs, different radio-emitting mechanisms and wavebands are relevant for studying material on different physical scales (e.g., Feigelson & Montmerle 1999; Güdel 2002): thermal dust emission from envelopes/disks (~200–10000 au scales); thermal bremsstrahlung from the base of partially ionized jets (~200 au scales); and gyro-emission from magnetic structures linking the YSOs to their disks ($\lesssim$0.5 au scales). In at least one confirmed case, nonthermal (synchrotron) emission is also seen from jets on pc scales (as indicated by linearly polarized emission, Carrasco-González et al. 2010), but its presence is strongly suspected in additional sources (e.g., Rodríguez-Kamenetzky et al. 2016; see also Section 4.3).

The typical radio spectrum of a low-mass YSO is dominated by thermal bremsstrahlung at frequencies below ~50 GHz and thermal dust emission at higher frequencies. However, Loinard drew attention to IRAS 16293–2422, whose "B" component has a spectral energy distribution (SED) that can be fit with a single steep power law ($\alpha \approx 2.3$) all the way from 2.5–690 GHz. The source size increases at lower frequencies, implying the emission dominated by dust even at cm wavelengths (for free–free emission, the opposite trend would be expected), implying this YSO is in a very early accretion stage. Data from the Atacama Large Millimeter/submillimeter Array (ALMA) were able to resolve for the first time an inverse P Cygni line profile, implying strong infall and providing a rare glimpse into how the material is infalling at different positions along the envelope (J. Hernandez et al. 2018, in preparation).

Recently, the ALMA Partnership et al. (2015) resolved the disk of the young, solar-type star HL Tau at mm and submm wavelengths into a spectacular series of rings and dust structures that have been interpreted as evidence for ongoing planet formation. However, Loinard noted that the region inside 10 au (where terrestrial planets are expected to form) is optically thick at ALMA bands. Fortuitously, the disk becomes optically thin at 7 mm, which allowed Carrasco-González et al. (2016) to undertake a comprehensive investigation of the inner disk using the Karl G. Jansky Very Large Array (VLA) at an angular resolution comparable to ALMA's. This underscores the complementarity of longer wavelength facilities for the study of planet formation. Loinard noted that a next-generation VLA (ngVLA; Murphy et al. 2018) would enable even more detailed studies of individual gas clumps and other features of the terrestrial planet-forming region of such sources.

4.2. New Constraints on YSO Masses

A longstanding problem with current models for low-mass PMS stars is a discrepancy between the predicted and empirically derived masses. Theoretical values are systematically too low by ~10%–30% (e.g., Hillenbrand & White 2004), and the disagreement becomes worse for lower-mass objects. R. Azulay (Max Planck Institut für Radioastronomie)

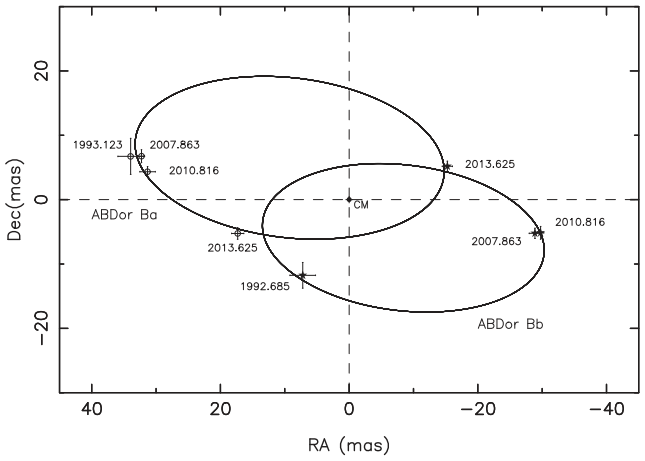

Figure 1. Absolute orbits of components "a" and "b" of the PMS binary system AB Dor B, obtained from IR data (circles) and VLBI astrometry spanning roughly 6 years (star symbols). The resulting mass determinations of the individual stars support the existence of a still unexplained discrepancy between empirical and theoretical masses for low-mass PMS stars. From Azulay et al. (2015), reproduced with permission © ESO.

described an effort to obtain an empirical calibration for mass models by using multi-epoch astrometry from very long baseline interferometry (VLBI) to derive dynamical masses for binaries within the AB Dor moving group. Observations of the binary AB Dor B were conducted with the Australian VLBI network at 8.4 GHz during three epochs spanning roughly 6 years (Azulay et al. 2015; Figure 1). A second AB Dor binary, HD 160934, was observed at 5 GHz using the European VLBI Network (EVN) during three epochs spanning 18 months (Azulay et al. 2017b). In both cases, radio (synchrotron) emission was detected from the two binary components, and the dynamical mass estimates derived from orbital fitting are systematically higher by 10%–40% than predicted by theoretical H-R diagrams for PMS stars, consistent with previous trends. Azulay suggested that the most likely explanation is inadequate treatment of convection in the models. Further astrometric studies by Azulay and collaborators are targeting additional stars and brown dwarfs (Azulay et al. 2017a; Guirado et al. 2018).

4.3. Radio Emission from the Jets of YSOs

Historically, the study of free–free emission from thermal jets has been one of the most important applications of radio observations to the study of YSOs (see review by Anglada et al. 2018). Typically, this emission arises from the base ($\lesssim$100 au) of large-scale optical jets. Most theoretical models predict that these jets are accelerated within the central au, and there is a clear connection between accretion and ejection in the sense that the mass traced by the free–free jet emission should be proportional to the mass being accreted (modulo an efficiency factor of $\sim$10%). While this is largely born out by observations, Loinard noted that an important goal for future studies will be to systematically relate the knots frequently observed in YSO jets (assumed to arise from episodic ejection) with the accretion process in a given star.

Until now, YSO jets had been previously little explored at longer radio wavelengths and had not been detected below $\sim$1 GHz. However, R. Ainsworth (Jodrell Bank Centre for Astrophysics), has begun exploiting newly available low-frequency radio telescopes as a tool to more accurately constrain the physical properties of these jets and to facilitate the detection of nonthermal emission, if present. Ainsworth presented results from a pilot study performed with the Giant Metrewave Telescope (GMRT), as well as follow-up observations from the Low-Frequency Array (LOFAR).

The GMRT observations by Ainsworth's team targeted three bright, well-studied protostars in Taurus. All three were detected at both 325 and 610 MHz, and the SEDs are consistent with an extrapolation from higher frequencies where the emission is partially optically thin and characterized by a single power law (Ainsworth et al. 2016). However, for one source (DG Tau), nonthermal emission was also detected from a second radio component that appears to trace the shock front associated with a jet impacting the ambient medium. While synchrotron emission has been detected previously from at least one high-mass YSO jet (see Section 4.1), Ainsworth's finding is evidence that the jets of low-mass YSOs are also capable of accelerating material to relativistic velocities, despite being relatively low powered. Ainsworth noted that the acceleration most likely stems from the Fermi mechanism (diffusive acceleration), whereby charged particles systematically gain energy through repeated reflections (e.g., Padovani et al. 2015). Taking the measured radio luminosity from DG Tau, equipartition implies that a minimum magnetic field strength of $\approx$0.11 mG and a minimum energy of $\approx 4 \times 10^{40}$ erg are required (Ainsworth et al. 2014). Ainsworth pointed out that jets of this type will be a source of Galactic cosmic rays, as the associated electron energies are estimated to be $\gtrsim$1 GeV.

Ainsworth reported that T Tau was also detected in follow-up observations at 150 MHz with LOFAR, marking the lowest frequency at which a YSO has ever been detected (Coughlan et al. 2017). The object was partially resolved, with hints of extension in the direction of a known large-scale outflow. A turnover of the SED from the higher-frequency power law was detected for the first time, thus breaking the degeneracy between emission measure and electron density and enabling unique determinations of these parameters, along with the ionized gas mass. Ainsworth and her collaborators are continuing efforts to characterize a larger sample of low-mass YSOs at low frequencies using both LOFAR and the GMRT, and these efforts are expected to benefit from recent GMRT sensitivity improvements.

4.4. Do YSOs Obey the Güdel-Benz Relation?

S. Wolk (Harvard-Smithsonian Center for Astrophysics; hereafter CfA) provided an update on a joint VLA-*Chandra* program on which he first reported at RS-1. This effort, led by J. Forbrich (University of Hertfordshire), was begun as a means of testing whether YSOs adhere to the Güdel-Benz (GB) relation, a tight power-law correlation between the radio (gyrosynchrotron) emission and X-ray luminosity spanning over 10 orders of magnitude that holds for wide variety of active stars (Güdel & Benz 1993; Benz & Güdel 1994). Whether it holds for YSOs can provide insights into high-energy processes in young stars, including the early, intense irradiation of protoplanetary disks.

The project described by Wolk has been taking advantage of the sensitivity of the upgraded VLA, combined with *Chandra*, to test whether the GB relation holds for hundreds of young stars in clusters. Early findings showed almost none of the YSOs being detected in the radio adhered to the GB relation; instead, the majority of stars detected in both bands were brighter in the radio than predicted (Forbrich et al. 2011; Forbrich & Wolk 2013). To ensure that these results were not biased because of sensitivity limitations or the lack of contemporaneous data, Wolk and Forbrich's team began a joint *Chandra*/VLA survey of the Orion Nebula Cluster comprising ∼30 h of coordinated radio/X-ray observations. In total, they detected 556 compact sources—a factor of seven increase in the number of radio sources in the region compared with past works (Forbrich et al. 2016b). Dual frequency measurements (4.7 and 7.3 GHz) permitted radio SED determinations. Only 112 of the sources are detected in the near-infrared (NIR) as well as in radio and X-rays, while 171 of the radio sources have no NIR or X-ray counterpart. In addition, 13 radio sources with extreme variability were identified, exhibiting more than an order of magnitude variation on timescales of less than 30 minutes; all are X-ray sources, but only a subset shows X-ray flaring on comparable timescales (Forbrich et al. 2017).

Obtaining a comprehensive understanding of these results remains an ongoing challenge. As noted by J. Linsky, the GB relation likely depends on a spatial correlation between two different parts of the electron energy distribution: thermal electrons (sampled by the X-rays), and nonthermal electrons (sampled by gyrosynchrotron radio emission). However, in the data shown by Wolk, the Hα, NIR, radio, and X-ray emission could be coming from different parts of a given object (jets, wind, proplyds, etc.). Some new insights are expected to come from follow-up VLBI observations presently being carried out for all 556 of the detected Orion sources (J. Forbrich et al. 2018, in preparation).

5. Radio Emission from Cool Dwarfs

5.1. Winds from Solar-like Stars

While the "coronal" winds from low-mass main-sequence stars typically produce only low rates of mass loss ($\sim 10^{-14}\,M_{\odot}\,\mathrm{yr}^{-1}$; Section 9), J. Linsky reminded us that these winds nonetheless affect the star's evolution by slowing rotation and altering angular momentum, and as a consequence, by changing the dynamo and magnetic field. However, a problem for studying coronal winds in the radio is the difficulty in distinguishing photospheric and chromospheric emission from wind emission. The frequency at which wind becomes optically thick depends on mass-loss rate and the assumed wind temperature and speed, but typically gyrosynchrotron emission will dominate over the wind at lower frequencies (cm wavelengths), while in the mm domain, the chromosphere dominates. Linsky emphasized that unambiguously detecting and disentangling these components poses a significant challenge. As evidence, he pointed to recent VLA observations of solar-mass stars where either the stars were undetected (Fichtinger et al. 2017), or where chromospheric emission was seen, but the data could not constrain the possibility of an additional coronal contribution to the radio flux (Villadsen et al. 2014). Linsky argued that new approaches will be crucial, such as observations with wider wavelength coverage, including mm wavelengths where there is no nonthermal emission component and where the chromospheric brightness temperature becomes weaker.

Another unknown for solar-type stars is the degree of constancy of their winds. Linsky pointed to work by Osten & Wolk (2015), who computed the expected time-averaged transient mass loss in coronal mass ejections (CMEs) for stars, taking into account an equipartition between the kinetic energy in the CMEs and the bolometric flux from a stellar flare. These results predict high mass-loss rates for stars like the young Sun or active M dwarfs—much larger than the current solar mass-loss rate. However, testing these predictions will require unambiguous detections of CMEs from other stars, which is something that has not yet been done (see Section 5.3).

5.2. Chromospheres

Linsky noted that the study of chromospheres in the ultraviolet (UV) or X-rays requires the observation of emission lines formed in non-local thermodynamic equilibrium (non-LTE) conditions over a range of temperatures. Furthermore, different portions of the emission line form in different parts of the atmosphere, making it necessary to solve the radiative transfer equation. In comparison, radio wavelengths offer a number of advantages for studying the thermal structure of the same star. The dominant emission process is free–free continuum for which LTE conditions hold (e.g., Wedemeyer et al. 2016). Opacity in the radio is simple and well understood

(electron-ion and H^- free–free), and heating rates can be derived empirically. Radio brightness temperatures can be derived from a simple integral of electron temperature over height, whereas temperatures in the UV require a more complex integration over a source function with height, which is not related to the Planck function (as in the radio), but rather to the statistical equilibrium distribution of the Planck function times the departure coefficient. In the radio, the free–free emission from longer to shorter wavelengths successively probes the photosphere to upper chromosphere, whereas in UV lines, the photosphere contributes to the emission line wings, the chromosphere to the peak, and the transition region to the line core. Finally, circular polarization of the mm continuum can trace variations in electron densities (e.g., White et al. 2017; Loukitcheva et al. 2017; see also Section 8.3) and provides one of the best available means to measure chromospheric B-fields.

Linsky additionally pointed out that radio observations are likely the best means to resolve the longstanding question of whether A- and B-type stars (which lack convective zones) have chromospheres. Chromospheres are difficult to measure in the UV for warmer stars because of the increasing contamination from the photosphere, but radio measurements may provide some new insights.

5.3. Activity on Cool Dwarfs

The study of stellar flaring at radio wavelengths has long been relevant for understanding the magnetic properties of stars and uncovering the similarities and differences between their magnetic activity and the Sun's. More recently, this topic has seen a dramatic surge in interest owing to its relevance to assessing exoplanet habitability (see Section 7). Not surprisingly, studies of stellar activity received proportionally far greater attention at RS-2 than RS-1 (cf. Matthews 2013). The present section focuses on meeting content related to active stars and binaries earlier than spectral type M7; activity on UCDs (Section 6) and the Sun (Section 8) are described separately. However, there was naturally thematic overlap, and one outstanding question is whether the type of large-scale magnetospheric currents now inferred in UCDs may also be present in some other classes of active stars (see Section 6).

As discussed by S. White (Air Force Research Laboratory) and R. Mutel (University of Iowa), the bulk of the radio emission observed from active stars at cm wavelengths is nonthermal gyrosynchrotron radiation arising from a power-law distributions of highly relativistic electrons in the corona, thought to be produced from flare acceleration and/or magnetic reconnection events. Evidence for this interpretation comes from the polarization properties of the emission, as well as VLBI observations of active stars where $T_B \sim 10^9$ K is observed. Unfortunately, the harmonics are highly broadened in this regime, thus as pointed out by White, it is not possible to identify a specific magnetic field strength with a specific emission frequency. Mutel and White therefore discussed, respectively, the feasibility of gleaning insights through the study other flavors of radio emission from active stars, namely thermal gyrosynchrotron and gyroresonance.

5.3.1. A First Detection of Thermal Gyrosynchrotron Emission Beyond the Sun

In hot plasmas displaying nonthermal gyrosynchrotron emission, thermal gyrosynchrotron emission may also arise from the Maxwellian tail of a thermal electron density distribution (e.g., Dulk 1985). Predicted observational signatures are deviations in the SED from a pure power law, along with very high fractional circular polarization (~30%–100%). R. Mutel recounted his recent efforts to search for thermal gyrosynchrotron from eight radio-loud stars selected from different parts of the H-R diagram. The optical depth of thermal gyrosynchrotron, τ_ν, is strongly dependent on both the magnetic field strength B and the temperature T ($\tau_\nu \propto T^7 B^9$). Given these strong dependencies, this emission is not expected to be detectable unless $T \sim 10^8$ K and $B \sim 1$ kG (i.e., the plasma is very hot with a very strong magnetic field). Mutel's target sample therefore included three chromospherically active binaries, two PMS (weak-line T Tauri) stars, and three M dwarfs. Contemporaneous flux density measurements were obtained for each star at several frequencies between 15–45 GHz using the VLA.

Mutel found that the SEDs of the three active binaries showed no evidence for thermal gyrosynchrotron, appearing instead as power law sources consistent with nonthermal gyrosynchrotron. However, for the two PMS stars and the M-dwarf binary UV Ceti, compelling evidence for a thermal gyrosynchrotron component was identified based on the shape of the SED and the presence of enhanced circularly polarized emission above 30 GHz. Not surprisingly, these are the targets with the highest plasma temperatures. Mutel reported that this is the first time that evidence for thermal gyrosynchrotron emission has been seen from a star other than the Sun.

5.3.2. Gyroresonant Emission from Active Stars

In analogy with previous work on the Sun, a potential means of probing coronal magnetic field strengths in non-relativistic plasmas somewhat cooler (~10^6 K) than those targeted by Mutel (Section 5.3.1) is gyroresonance emission (White 2004). In particular, S. White evaluated the prospect of linear polarization measurements of such emission as a tool for understanding the magnetic properties of active stars. He concluded that in most cases, the combined signal from the two stellar hemispheres will dramatically reduce the overall amount of polarization, making it difficult to identify gyroresonance emission. An exception may occur in the case of stars with large polar spots viewed nearly pole-on. However, even in

these cases, there may be another complication uncovered by earlier work, namely that the presence of plasma emission at lower frequencies can confuse the interpretation of the gyroresonant emission, leading to an apparent polarization reversal between low and high frequencies (White & Franciosini 1995).

5.3.3. Time-domain Studies of Active Stars

Taking advantage of the frequency ranges now accessible with the Murchison Widefield Array (MWA), C. Lynch (University of Sydney) described an ongoing program to characterize the little-explored radio flares from M dwarfs that occur at frequencies of a few hundred MHz. This topic has received only scant attention since a few pioneering studies more than 30 years ago, where m-wave flaring was detected from 11 M dwarfs (Spangler & Moffett 1976; Davis et al. 1978; Kundu et al. 1988). Lynch noted that although this particular emission was recognized as being coherent, there has been an unresolved controversy as to whether the underlying mechanism is plasma or ECM emission.

Previous statistics on the strength and frequency of "MHz" flares, coupled with the known presence of >2000 M dwarfs in the Southern Hemisphere within 25 pc (Winters et al. 2015) led to the prediction that M-dwarf flares should be ubiquitous in transient surveys conducted by modern low-frequency instruments like the MWA. Surprisingly, no flaring M dwarfs were detected in two recent widefield MWA surveys (Tingay et al. 2016; Rowlinson et al. 2016). To better understand why, Lynch and her colleagues began deeper targeted observations of M dwarfs to characterize their behavior at meter wavelengths. The observations emphasized Stokes V (circular polarization) data products to overcome the confusion limits that otherwise plague deep integrations at MWA frequencies, effectively boosting the achievable sensitivity by a factor of ∼80.

Using this approach, Lynch et al. (2017) reported a detection of flaring from UV Ceti in each of four days when the star was observed with the MWA, marking the first detection of meter-wavelength flaring from an M dwarf with current-generation radio facilities. The emission is coherent, and a signature of linear polarization was observed from the brightest flare, indicating that the emission is elliptically polarized and hence is likely to be ECM (Figure 2). This finding permitted an estimation of the magnetic field strength at the location of the event (∼28 G). In addition, evidence for a periodicity of 5.45 hours was seen, echoing a behavior recently seen at higher frequencies (see below). However, follow-up observations by Lynch and colleagues in late 2017 did not detect this signal, indicating that it is not persistent. Two other targeted M dwarfs, YZ CMi and CN Leo, were undetected at the time of the meeting, but MWA observations remain ongoing. Lynch stressed that information on flare rates and luminosities at

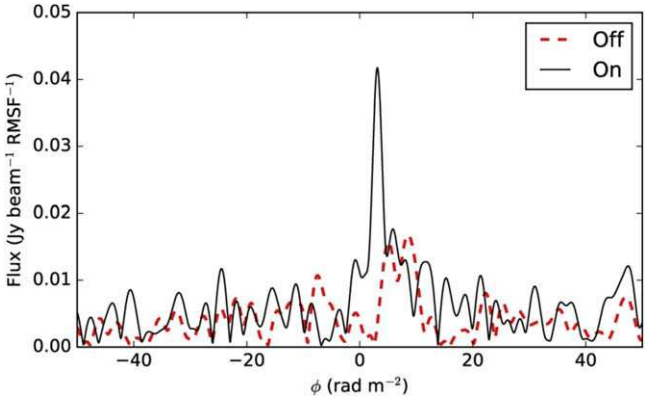

Figure 2. Faraday dispersion function during a bright flare on the active star UV Ceti (black curve), derived via rotation measure synthesis from 154 MHz MWA data. The implied linear polarization fraction is >18%, suggesting that the emission arises via an ECM mechanism. No linearly polarized emission was detected during an adjacent non-flaring interval (red dashed line). Reproduced from Lynch et al. (2017). © AAS.
(A color version of this figure is available in the online journal.)

m-wavelengths remains extremely limited and that significant amounts of dedicated observing time with low-frequency telescopes will be needed to improve these statistics. She noted that unfortunately computational limitations currently preclude the routine mining of data from other MWA experiments for M dwarf flare events.

Another recent campaign aimed at studying activity on M dwarfs, but at somewhat higher frequencies, is being led by J. Villadsen (National Radio Astronomy Observatory; hereafter NRAO). A primary underlying motivation is understanding the extrasolar space weather associated with these stars (see also Section 7.2), and in particular whether they are subject to CMEs. Villadsen emphasized that while flares are observed frequently from M dwarfs, CMEs and energetic protons are not; they are only predicted.

The detection of CMEs from stars other than the Sun has been a longstanding quest for astronomers, but so far no such events have been unambiguously identified (see also Section 7.2). While coherent bursts of emission from M dwarfs sometimes exhibit frequency drifts reminiscent of solar CMEs, as with the m-wave emission discussed by Lynch (see above), it has so far remained impossible to differentiate between coherent plasma emission (as occurs with solar CMEs) and ECM emission. Furthermore, as noted by Osten, it has so far proved difficult to identify an observational signature that can be ascribed uniquely to CMEs and not to flares.

In hopes of making progress in this quest, Villadsen and her colleagues used the VLA to study a sample of five M dwarfs over 22 epochs in bands covering 0.22–0.48 GHz and 1–4 GHz (or 1–6 GHz). Their goal is to identify events with a time-frequency evolution analogous to solar CMEs. Having multiple frequency bands allows tracing plasma at different distances

from the star, with the higher frequencies probing the low corona and the lower frequency band probing ∼1.5–3 $R_\star$. This arises from the dependence of the radio-emitting frequency on the electron density and magnetic field strength at a given height (e.g., Dulk 1985). In parallel, Villadsen's team used the Very Long Baseline Array (VLBA) to attempt to resolve the radio coronae before and after flares. While it is known from previous VLBI experiments that the radio corona of M dwarfs can become extremely extended during periods of activity (e.g., Benz et al. 1998), Villadsen's study is the first attempt to connect high-resolution VLBI imaging with wide bandwidth dynamic spectroscopy (Villadsen et al. 2017).

The VLA data obtained by Villadsen and collaborators helped to confirm that coherent bursts in M dwarfs are extremely common, occurring in 13 of 22 observed epochs and on a variety of timescales, from seconds or minutes to events lasting an hour or longer. The latter require some type of persistent electron acceleration process which Villadsen suggested may be emerging magnetic flux driving magnetic reconnection over extended intervals, analogous to what happens on the Sun.

However, while tantalizing hints of CME-*like* phenomena were seen in some objects, unambiguous signatures of a CME remain elusive. For example, in AD Leo, an off-limb flare was observed with the VLBA, nearly a full stellar diameter from the star, but the dynamical spectrum taken with the VLA at the same time shows no evidence of outward motion and no obvious connection with this event. In the case of UV Ceti, dynamic spectra from five different epochs all show very similar structures, suggesting some kind of periodic phenomenon that could be related to the periodicity seen at meter wavelengths (see above). Some features in the UV Ceti data exhibit a frequency drift with time, but Villadsen argued that the emission is more likely analogous to the periodic aurorae seen in UCDs and planets (see Section 6) and therefore attributable to an ECM mechanism, not plasma emission from a CME. In the ECM scenario, frequency drift results from geometric modulation rather than motion of blobs of material.

Campaigns reported by other meeting participants had similar outcomes. For example, R. Osten (Space Telescope Science Institute) described recent VLA measurements of EQ Peg at 230–470 MHz, performed with simultaneous near-UV monitoring. In 20 hours of data, several moderate flares were seen, but no "type II" events (see also Section 8.1) of the kind expected to occur along with CMEs (Crosley & Osten 2018).

The confluence of these results naturally leads to the question: why do we not see CMEs from other stars? One possibility raised by Osten is that perhaps CMEs are not super-Alvfénic, hence no shocks are produced. Two additional possibilities suggested by B. Chen (New Jersey Institute of Technology) are that either the ejected material is very clumpy or else that the brightness temperature of the type II radio burst cannot become sufficiently high before their electromagnetic energy is converted back into Langmuir waves. Osten also noted that a related question that merits further study is whether the large magnetic field strengths of M dwarfs might prevent the magnetic breakout needed for the ejection of material from the stellar surface. This question is particularly relevant for the question of exoplanet habitability (Section 7.2).

5.3.4. Insights into Solar and Stellar Activity from Theory and Modeling

As the quality of radio observations of active phenomena on the Sun and other stars grows, so does the need for increasingly sophisticated theoretical models to aid in the physical interpretation of the data. S.-P. Moschou (CfA) described a new state-of-the-art tool that is capable of producing realistic radio synthetic images of both quiescent and transient phenomena over a wide range of radio wavelengths. The models incorporate a variety of important physics, including acceleration, scattering, and shocks. Because radio waves from a star like the Sun are highly refracted, the curvature of the ray paths must also be treated to properly compute the emergent radio intensity in each pixel of the model images (see Benkevitch et al. 2010).

Moschou presented first results from applications of her code to the study of radio-loud CMEs and their relationship to other transient phenomena on the Sun. The resulting models capture the CME shock wave and allow watching the development of an ensuing type II radio burst. Future work by Mochou's team will include adding the treatment of polarization and magnetic fields in their code, as well as application of the code to other stars.

5.3.5. Future Directions for Radio Studies of Active Stars

J. Linsky suggested several ways of obtaining crucial new physical insights into active stars. He argued for further work in the mm domain, noting that (sub)mm monitoring over several rotation periods might help to reveal periodic flux density modulations indicative of the presence of hotter regions or cooler starspots. Commensal studies of flares in (sub)mm and hard X-rays are also expected to be fruitful (see Krucker et al. 2013), as both bands show the same thermal structure in flares, though soft X-rays show a more gradual development. Linsky also advocated for expansion of the spectral types targeted for flare studies. While typical radio observations of M dwarfs routinely lead to flare detections within a few hours of integration, active G stars with strong optical flaring (∼100–1000 times typical solar flare luminosities) have been discovered with *Kepler* (e.g., Katsova & Livshits 2015) and would be interesting targets for future studies. In addition, Linsky stressed the desirability of combining multiple radio instruments (e.g., the VLA and ALMA) to observe flares from various types of stars simultaneously from cm to mm

wavelengths, as this could provide important insights into the distribution of the relativistic electron energies. He cited previous work by Raulin et al. (2004) that looked at how the frequency of the peak in the gyrosynchrotron emission changes with time in solar flares and noted that this has yet to be studied for other stars. Finally, Linsky raised the prospect of whether Doppler imaging might soon become possible for active stars at radio wavelengths. As a step in this direction, A. Richards (Jodrell Bank Centre for Astrophysics/University of Manchester) noted that she and her colleagues have already produced a spatially resolved velocity field for the red supergiant Betelgeuse using data from ALMA (Kervella et al. 2018).

6. Emission from Ultracool Dwarfs (UCDs)

6.1. The Origin of the Radio Emission

As described in the review by G. Hallinan (California Institute of Technology), the past few years have seen significant progress toward a comprehensive picture of activity on UCDs (i.e., stars with spectral types $\gtrsim$M7; see reviews by Pineda et al. 2017; Williams 2017). The ultra-wide bandwidths provided by the VLA and other current-generation radio facilities have been instrumental in the recent growth of this area, and not surprisingly, this topic received considerable attention at RS-2.

Hallinan reminded us that the radio emission from UCDs is characterized by both "quiescent" emission (including flares; Section 6.3), as well as periodic, pulsed emission that is highly ($\sim$100%) circularly polarized (e.g., Hallinan et al. 2006, 2007). Frequently, radio-detected UCDs are rapid rotators, and the periodicity of the pulsed emission component is found to be closely tied to the stellar rotation period (typically a few hours), consistent with rotational beaming. The high inferred brightness temperature of the pulsed emission, coupled with its strong circular polarization, points to a coherent emission mechanism that is now attributed to ECM.

The atmospheres of UCDs are sufficiently cool to become largely neutral, allowing the magnetic field to become decoupled from the photospheric gas. Consequently, processes like magnetic reconnection no longer dissipate significant amounts of energy. This transition is found to correspond to a marked departure from the domain of coronal/chromospheric magnetic activity to planet-like auroral magnetic activity. Importantly, in this regime currents are driven by a global electrodynamic interaction in a large-scale magnetic field instead of local photospheric plasma motions (see Pineda et al. 2017).

A recent radio and optical study of the M9 dwarf LSR J1835 +3259 by Hallinan's team led to a simple, unifying model to explain the radio, Hα, and broadband optical emission through an electron beam powered by auroral currents (Hallinan et al. 2015). In this model, as the electron beam hits the upper atmosphere, a supply of free electrons leads to the production of H^-, whose opacity then dominates high in the atmosphere. This results in regions that are cooler than the surrounding photosphere and produces a largely blackbody spectrum (corresponding to $T_B = 2180$ K)—very different from a pristine photospheric spectrum, which is dominated by molecular absorption.

Hallinan emphasized that the aurorae of relevance to UCDs are quite different from those observed terrestrially. The latter are dominated by a mechanism whereby the solar wind interacts with Earth's magnetosphere, producing acceleration of electrons along magnetic field lines (Pineda et al. 2017 and references therein). These events are a byproduct of local and impulsive current systems on the Sun, driven by reconnection events or shock fronts (see Section 8). In contrast, UCDs have large-scale current systems that are global and quasi-stable and that are thought to power aurorae through energy dissipation (see also Section 6.2). Hallinan stressed that it remains an open question as to whether a similar type of large-scale magnetospheric currents may also occur in other classes of stars that display pulsed emission and evidence for large-scale magnetic fields (see Sections 5.3 and 10.1.4).

One lingering puzzle pointed out by Hallinan is why only a small fraction of brown dwarfs ($\sim$7%–10%) are detected in sensitive radio searches. One potential clue is a dependence on rotation velocity, with a higher rate of detection for the rapid rotators (Pineda et al. 2017), raising the possibility that there exists a critical rotational velocity to achieve co-rotation breakdown. The low detection statistics have until recently thwarted attempts to better characterize the magnetic field strengths and underlying electrodynamic engine of brown dwarfs (see below). However, as discussed by M. Kao (Arizona State University), the auroral nature of the brown dwarf radio emission results in a correlation between characteristic time-varying emission in the Hα line and the IR continuum (Hallinan et al. 2015). These latter tracers have now been shown to serve as an effective proxy for the identification of radio-bright brown dwarfs (Kao et al. 2016; Section 6.2).

6.2. Origin and Characterization of Magnetic Fields on UCDs

One of the chief outstanding challenges for the auroral model of radio emission from UCDs is to explain the generation and maintenance of the persistent magnetic fields in these fully convective stars. Mechanisms that may plausibly generate aurorae in isolated UCDs are (1) the occurrence of a co-rotation breakdown when the field further out becomes too weak to drag along the plasma, and (2) the presence of an embedded object within the UCD magnetosphere (Trigilio et al. 2018; see also Section 7.3). Presently, no conclusive evidence exists to favor either mechanism, but both require the presence of persistent UCD magnetic fields. UCD magnetic field measurements based on radio data (e.g., Route & Wolszczan 2012; Kao et al. 2018),

along with magnetic field topological modeling and comparisons with radio dynamic spectra may help to provide new insights (e.g., Lynch et al. 2015; Leto et al. 2016).

Zeeman Doppler measurements are traditionally used to characterize the magnetic fields of low-mass, magnetically active stars (Semel 1989), but this technique breaks down for spectral types cooler than ∼M9. However, ECM emission is produced at or close to the fundamental cyclotron frequency ($\nu_{\rm MHz} \approx 2.8 \times B$, where B is the magnetic field strength in G; Treumann 2006), making it a unique and powerful tracer of the local field strength in radio-bright UCDs (Hallinan et al. 2008; Route & Wolszczan 2012), provided that the plasma densities are sufficiently low (see Mutel et al. 2006). Despite this, magnetic field measurements for L, T, and Y dwarfs have until recently remained sorely lacking owing to the challenge of identifying suitable radio-emitting targets. However, M. Kao presented results for a new sample of six brown dwarfs observed with the VLA in the 4–8 GHz band. The objects were selected based on their IR and Hα variability (see Section 6.1). Highly circularly polarized emission was detected from five of the six, including one previously observed T6.5 dwarf (Kao et al. 2016). Follow-up observations of the sample in 8–12 GHz and 12–18 GHz bands showed tentative evidence that the auroral radio emission at these higher frequencies starts to become more variable, but two IR-variable Y dwarfs were not detected. The future radio detection of Y dwarfs would be helpful in probing a temperature range where there currently exists no constraints on magnetic fields, although such detections may be beyond the sensitivity limits of current instruments.

Kao pointed to previous work by Christensen et al. (2009) showing that a scaling of the convection-driven dynamo found in planets such as Earth and Jupiter appears to account for the magnetic fields of low-mass stars, suggesting a single, unified mechanism governing magnetic activity in all rapidly rotating, fully convective objects over more than three orders of magnitude in field strength. However, Kao's latest results appear to deviate from the Christensen et al. relation. Accounting for age- and temperature-related effects, including the decay or magnetic fields with time, does not remove this discrepancy (Kao et al. 2018). J. Linsky pointed out that very young brown dwarfs may still be burning deuterium, leading to very different interior structures compared with older brown dwarfs.

6.3. Quiescent Radio Emission from UCDs

Another outstanding puzzle concerning UCDs is the nature of their quiescent radio emission seen at GHz frequencies. Such emission is ubiquitous in UCDs with pulsed radio emission and is observed to show variations over a wide range of timescales, including flare-like activity (e.g., Route 2017). Hallinan noted that it is presently unknown whether the same current system powers both the pulsed and quiescent emission, and P. Williams (CfA) highlighted the shortcomings of existing models for describing recently observed radio spectra. For example, while the quiescent emission is generally thought to be gyrosynchrotron in nature, recent ALMA observations of the UCD NLTT 33370 AB at ∼100 GHz by Williams (P. Williams et al. 2018, in preparation) show a surprisingly high level of circular polarization (∼30%), posing a possible challenge for this model (see Williams et al. 2015; but cf. Section 5.3.1).

Williams proposed a "van Allen belt" model for the quiescent emission from UCDs, whereby energetic particles become trapped in a stable, dipolar magnetosphere very different from the magnetospheres of solar-type stars. He noted that this would go hand-in-hand with the auroral model discussed by Hallinan, which also requires a stable magnetosphere.

The van Allen belt model lends itself to a physically elegant description of charged particle motion, and Williams has begun developing sophisticated codes for the purpose of simulating radio (synchrotron) emission from van Allen belt-type structures under an open source project he calls "vernon".[3] Crucial pieces include solving the steady-state Fokker-Planck equation to get particle distributions in a 6D phase space (which includes energy and pitch angle of the particles) and then performing radiative transfer calculations to simulate the resulting emission distribution. Williams has built on the "symphony" code of Pandya et al. (2016) by incorporating ingredients necessary for the proper treatment of the planetary radiation belt problem, including anisotropy in the radiative transfer and routines to calculate Faraday coefficients. Williams presented initial results from his code as applied to the Jovian system, demonstrating that the results appear quite promising.

Recent efforts to detect flare-like emission from UCDs at moderately low frequencies were described by A. Zic (Univ. Sydney). Zic's ongoing study focused on two well-studied objects for which he obtained 0.6 and 1.0 GHz observations with the GMRT: the late M dwarf TVLM 513-46, and the M7 binary LSPM J1314+1320. Assuming that the quiescent radio emission (including flares) from these two stars is gyrosynchrotron in nature (McLean et al. 2011; Lynch et al. 2015), detection of a low-frequency turnover beyond which the radio emission becomes optically thick is expected to break the degeneracy between magnetic field strength and number density in the flare-emitting region. Zic presented first results based on the 1 GHz data. TVLM 513-46 was undetected, but LSPM J1314+1320 exhibited both quiescent emission (∼1 mJy) and short-duration (<1 minute) flaring that peaked at ∼5 mJy. These represent the lowest frequency and shortest duration burst detected from this system to date.

[3] https://github.com/pkgw/rimphony

6.4. Mass Measurements of Brown Dwarfs

Direct mass measurements are crucial for constraining evolutionary models of brown dwarfs. As highlighted by Hallinan, VLBI observations of the radio emission from binary brown dwarfs are playing a crucial role in providing dynamical masses (Dupuy et al. 2016; Forbrich et al. 2016a). These measurements are unique, as most of these sources are too faint to be observed by *Gaia*, and adaptive optics measurements in the IR can yield on only relative motions, leading to a degeneracy in the masses of the individual components.

7. Radio Emission from Exoplanets and their Host Stars

7.1. Direct Radio Detections of Exoplanets

While by design the RS-2 meeting was focused primarily on the study of stellar radio emission rather than exoplanet searches and characterization, G. Hallinan remarked that radio searches for exoplanets are expected to be one of the next major frontiers in astrophysics. The many low-frequency (<300 MHz) arrays coming on line are poised to aid in these quests, although detection of Jupiter-like objects will likely remain challenging prior to the availability of the Square Kilometer Array (SKA). Nonetheless, detections are possible, since as noted by C. Lynch, models predicting the radio fluxes are still poorly constrained. Furthermore, the first (free-floating) exoplanet may have already been detected in the radio. M. Kao and collaborators (Kao et al. 2016, 2018; Section 6) recently detected a UCD whose derived mass of $\sim$13 $M_{\rm Jupiter}$ (Gagné et al. 2017) places it near the boundary between brown dwarfs and exoplanets. M. Anderson pointed out that ultimately the best place to detect exo-Jupiters will be from space, where it is possible to access frequencies below the ionospheric cutoff ($\lesssim$10 MHz)—the best realm for detecting magnetic fields analogous to those of solar system objects.

7.2. Extrasolar Space Weather

The recent discoveries of rocky planets surrounding cool and ultracool stars (e.g., Dressing & Charbonneau 2015; Gillon et al. 2017) naturally leads to speculation about the habitability of these bodies. This question has captivated not only astrophysicists, but also the public, and is one where radio astronomy is poised to play a key role. Indeed, R. Osten noted that this has been a major force in reinvigorating interest in studies of stellar magnetic activity at radio wavelengths (although they are often reframed in terms of understanding how a star might influence its environment). This topic is commonly referred to as "extrasolar space weather," although J. Linsky pointed out that extrasolar space weather often refers to the sum total of events that affect planets over their lifetimes, making it more akin to "climatology" than "weather."

As noted by Linsky, Osten, and other speakers, the question of exoplanet habitability goes far beyond the presence of liquid water, to matters such as the importance of CMEs (which may compress planetary magnetospheres, exposing their atmospheres to erosion) and whether various energetic processes (flares, ionized winds, pick-up processes, UV heating, and sputtering) might destroy ozone and otherwise impact the atmospheric chemistry of planets (e.g., Osten & Crosley 2017; Airapetian et al. 2018). And importantly, not only do many late-type stars have significantly higher activity levels than the Sun (e.g., Shibayama et al. 2013; Karmakar et al. 2017), but as J. Villadsen reminded us, they may stay highly active for up to several Gyr, in contrast with the Sun, where activity levels fall steeply within a few hundred Myr past the zero age main sequence (see Guinan & Engle 2009).

In her review of extrasolar space weather, Osten noted that if one makes the assumption that CMEs accompany flares, an implication is that low-mass stars must incur a very large mass-loss rate due to CMEs. This would dramatically impact habitability, because not only are potentially habitable M dwarf planets closer to their host stars than the Earth is to the Sun, but they also will likely be tidally locked and may possess a weak magnetic moment, providing little magnetospheric protection from CMEs (Lammer et al. 2007). However, as discussed in Section 5.3, there have so far been no unambiguous detections of CMEs (or their associated high-energy particles) from other stars to support this hypothesis. Osten further pointed out that none of the hard X-ray flares that have been detected from other stars to date have been convincingly shown to be nonthermal in nature (Osten et al. 2016).

As a consequence of this present lack of direct CME measurements, researchers commonly resort to extrapolating properties of the Sun's flares to the low stellar mass regime in order to infer information on space weather and planet habitability. However, Osten warned that there is no compelling evidence that such scalings are valid (e.g., Osten & Wolk 2015). For example, previous work by Segura et al. (2010) showed that a typical UV flare will have only a $\sim$1% effect on the ozone layer of an earth-like planet. On the other hand, the same authors showed that the associated energetic particles (as scaled from solar events) would be sufficient to completely destroy the atmosphere of an Earth-like planet in the habitable zone of an M dwarf.

Osten further noted that while both solar and stellar flares have similar radiative energy partitions (i.e., similar ratios of radiative energy of flares to the total blackbody emission of the star; Osten & Wolk 2015), earlier work of Güdel et al. (1996) showed that stellar flares tend to produce stronger radio amplitudes relative to their X-ray emission than do solar flares. Subsequent studies have also found that solar eruptive events tend to have similar amounts of energy in radiation and energetic particles (as measured through X-rays; Emslie et al. 2012), while M dwarf flares tend to have a larger fraction

of energy in nonthermal particles (Smith et al. 2005). One positive step forward was recently made by Osten and her collaborators (Crosley et al. 2017), who in effect observed the Sun as an unresolved star to develop a framework for the interpretation of stellar events and the derivation of parameters such as CME velocities, masses, and kinetic energies.

In a parallel effort, M. Anderson (California Institute of Technology) described work underway with the Owens Valley Radio Observatory Long Wavelength Array (OVRO-LWA; Hallinan & Anderson 2017) to search for signatures of extrasolar space weather phenomena at frequencies where emission from type II burst-like emission and ECM emission from exoplanets are expected to peak ($\nu < 100$ MHz). The all-sky coverage of the OVRO-LWA is uniquely powerful in allowing it to simultaneously observe many objects and potentially catch rare events. Imaging in Stokes V also capitalizes on the the circularly polarized nature of the expected emission to improve the signal-to-noise ratio (S/N) at these low frequencies where confusion dominates the background (see also Section 5.3.2).

The survey by Anderson's team is targeting a volume-limited sample of more than 4000 nearby ($d \lesssim 25$ pc) stars spanning a range in spectral type to look for signatures of CMEs and radio emission from extrasolar planets (Anderson & Hallinan 2017). The sample includes >1000 L, T, and Y UCDs, 1300 M dwarfs, and other higher mass stars. A primary goal of this work it to gain a better understanding of how CMEs (and their impact on exoplanet habitability) scale with flare energy and frequency. Anderson's team also seeks to further test the suitability of scaling relations between flare flux with CME mass based on the Sun (see also above) by comparing with results inferred by assuming energy equipartition between the bolometric flare energy and the kinetic energy.

Observations by Anderson's team have been ongoing since 2016 November, and simultaneous optical monitoring is expected to provide critical information for tying together flares with radio emission linked to CMEs. When complete, the resulting survey will be equivalent to >5000 hours of targeted observations with sufficient frequency and time resolution to identify the types of frequency drifts that are characteristic of CME-associated type II bursts and plasma propagating out through the corona.

7.3. Effects of Exoplanets on their Stellar Hosts

A few speakers briefly touched on the possible influences exoplanets may have on the radio emission of their host stars. For example, J. Linsky highlighted recent mm observations of Fomalhaut's disk that exhibit the hallmarks of planetary interactions (MacGregor et al. 2017), and he cited the importance of ALMA for answering the question of at what stage of star formation Jupiter-like planets form (e.g., Ansdell et al. 2017). R. Osten also drew attention to the study by Bower et al. (2016), which was the first to detect radio emission from a non-degenerate star that hosts an exoplanet (in this case, a T Tauri star). She noted that future observations of this type may be a promising way of yielding insights into the magnetic interaction between stars and their planets.

In the case of UCDs (Section 6), one explanation discussed by G. Hallinan to account for the electrodynamic engine underlying the observed auroral-type emissions is the presence of an embedded planet within the dwarf's magnetosphere. However, compelling observational evidence for this model is presently lacking, and Hallinan noted that the brown dwarf TRAPPIST-1 (which has many associated rocky planets; Gillon et al. 2017), does not fit this picture (Pineda & Hallinan 2018).

7.4. Radio Stars as Beacons for the Study of Exoplanets

Observations of radio signals from spacecraft as they pass near bodies within our solar system have long been used as a means to study the atmospheres and magnetospheres of other planets. P. Withers (Boston University) considered the question of whether this technique could be extended to exoplanets, i.e., whether the observation of stellar radio emission that had passed through the atmosphere of an exoplanet could be used to probe exoplanet properties. Such an occurrence is expected to affect the amplitude, frequency, and polarization of the radio signal and could in principle be used to infer parameters such as the neutral density in the atmosphere, plasma density in the ionosphere and magnetosphere, and the magnetic field in the plasma environment (Withers & Vogt 2017). Withers is presently researching the most promising candidates for detecting such effects. S. Wolk pointed out that there may be applicable lessons from analogous investigations recently done in the X-ray (e.g., Wolk et al. 2017).

8. The Sun as a Radio Star

Radio emission from the Sun samples a wide variety of emission processes from both thermal plasma and nonthermal electrons. At least five different solar radio emission mechanisms have been observed, including bremsstrahlung, gyroresonance, gyrosynchrotron, and coherent emission in the form of ECM and plasma emission (e.g., Figure 4.1 of Gary & Hurford 2004). As pointed out by S. White, all five of these emission mechanisms produce circularly polarized emission, which provides additional diagnostic information. (In contrast, linear polarization is wiped out by Faraday rotation on the Sun, rendering it unobservable).

Radio observations of the Sun are in general not S/N limited. Until recently, they have been instead limited by other technological constraints. For example, dynamic spectroscopy of solar emission has been limited by the bandwidths and sampling rates of the available instruments, most of which lacked imaging capabilities. However, as was amply illustrated at the meeting, solar radio astronomy has entered an exciting

new era thanks to the latest generation of instruments capable of dynamic spectro-imaging with high time and spectral resolution and over ultra-wide bands.

8.1. The Sun at Low Frequencies

At frequencies below $\lesssim$1 GHz, solar emission is dominated by a combination of thermal bremsstrahlung and plasma emission, the latter of which is seen both at the fundamental and the second harmonic of the plasma frequency. As discussed by S. White, a number of puzzles remain concerning the observed properties of this low-frequency solar emission. For example, the fundamental mode of the plasma emission is predicted to be 100% circularly polarized, but this is not always observed. Furthermore, absorption is thought to be quite high near the fundamental mode, necessitating some kind of duct to get the fundamental emission to emerge rather than getting absorbed.

Fortunately, the latest generation of low-frequency observatories are revolutionizing our understanding of the meter-wave emission from the Sun, and C. Lonsdale (MIT Haystack Observatory) described the exquisitely detailed imaging at frequencies of 80–300 MHz that are possible with the MWA. The MWA is a powerful solar imaging telescope owing to excellent instantaneous monochromatic *u-v* coverage and high time and frequency resolution (e.g., Mohan & Oberoi 2017).

To date, many petabytes of solar data have been gathered with the MWA, but a hurdle to exploiting them has been the challenge of developing a robust and accurate reduction method (e.g., Lonsdale et al. 2017). As Lonsdale described, significant progress has now been made, resulting in solar images that reach a dynamic range of up to 75000:1, and efforts are underway to achieve this on a routine basis. In comparison, the best that has been achieved by other instruments at similar frequencies is ∼300:1. Despite their high dynamic range, the MWA images are still not thermal noise-limited, and the limiting factor is now thought to be ionospheric microstructures tens to hundreds of meters in size that produce phase fluctuations of a few degrees on long baselines.

Lonsdale reported that a handful of type II solar bursts have been captured by the MWA. A hallmark of these bursts is a slow drift to lower frequencies with time that is visible in dynamic radio spectra, and these events are of considerable interest because of their close link with CMEs (e.g., White 2007). The analysis of a 2014 September event has provided the most detailed spatial information on a type II event ever achieved (Lonsdale et al. 2017; D. Oberoi et al., 2018, in preparation). During this burst, both the fundamental and second harmonic of the plasma emission were recorded two minutes apart in 30 MHz bands centered at 90 MHz and 120 MHz, respectively. Different frequency channels within each band sample different plasma frequencies (hence different electron densities), revealing a significant amount of complex, fine-scale structure. Analysis of these data also showed that the fundamental and harmonic emission appear to originate from different spatial locations, implying systematic outward motion from the Sun. The S/N was sufficient to enable extraction of spatial information on scales of a few percent of the MWA's resolution, and the quality of the data enable high-fidelity imaging of every pixel in a dynamic spectrum (with time and frequency resolution of 0.5 s and 40 kHz, respectively).

For another type II burst, MWA data were analyzed following the disappearance of the event, leading to the detection of gyrosynchrotron emission from the associated, outwardly moving CME material. Further analysis of these data will include attempting to measure the linear polarization to characterize the magnetic field in the CME plasma (K. Kozarev et al. 2016, and in preparation).

Lonsdale also illustrated the power of the MWA for imaging other types of solar events, including type III bursts. The latter give rise to radio emission at the plasma frequency and its harmonics and are characterized by rapid drifts in frequency with time (e.g., White 2007). Multi-frequency imaging of one such type III event by McCauley et al. (2017) showed that the intensity profiles of the burst emission become spatially more extended at lower frequencies and are double-peaked. The explanation for this phenomenon is that the electron beams that are traveling along the magnetic field lines are separating (over a time span of ∼2 s) because of travel along diverging field lines.

Crucial to mining the enormous volumes of solar data generated by the MWA and other modern radio facilities used for dynamic spectro-imaging will be the assistance from automated feature identification algorithms. Lonsdale drew attention to recent work by Suresh et al. (2017), who used a wavelet-based approach to automatically identify and characterize the numerous weak and short-lived emission features (undetectable with previous instruments) that are found in typical MWA solar data. Such features appear to be ubiquitous even during times of low solar activity (see also Oberoi et al. 2011). At times of medium activity on the Sun, up to half of the total solar flux density within the MWA bands comes from the aforementioned "mini-flare" events (Sharma et al. 2018), and these are suspected to be of importance for coronal and chromospheric heating.

Another low-frequency solar imaging instrument that is under construction is the Radio Array of Portable Interferometric Detectors (RAPID), a project led by MIT Haystack Observatory (see Lonsdale et al. 2017 and references therein). RAPID will comprise an array of 50–70 small, portable, reconfigurable, fully independent stations with self-contained power and data storage. Its wide instantaneous frequency coverage and reconfigurable layout will make it ideal for imaging different types of solar emissions, surpassing even the MWA.

8.2. The Sun at Centimeter Wavelengths

B. Chen provided an overview of the Sun at $\nu \gtrsim 1$ GHz, where bremsstrahlung ($\nu \sim 1$–3 GHz) and gyromagnetic radiation processes ($\nu \gtrsim 3$ GHz) dominate. As at lower frequencies (Section 8.1), solar work in this domain has been revolutionized by the expansion in bandwidth and sampling rates of the available instrumentation and the ability to perform exquisitely detailed dynamic spectro-imaging.

Chen drew attention to the recent commissioning of the only dedicated solar radio observatory currently operating in the United States, the Expanded Owens Valley Solar Array (EOVSA). It offers a usable frequency range of ~2.5–18 GHz (Gary et al. 2017) and it sweeps this entire range once per second. While its relatively small number of antennas (14) do not provide outstanding snapshot imaging capabilities, its broad frequency coverage and dedicated solar coverage are key advantages.

Chen described recent work using EOVSA to observe the Sun during the impulsive energy release phase of a 2017 X8.1 X-ray flare (Gary et al. 2018). The resolving power of the array was sufficient to reveal a reservoir of hot electrons lying on top of the coronal loops imaged in the extreme UV, and the broad spectral response confirms gyrosynchrotron emission spanning from 3–18 GHz. The EOVSA data enabled studying the time-varying SED of this emission (Figure 3), and fits to the spectrum to yield the magnetic field strength and electron density. The peak frequency of the emission decreases as material moves from low altitude to high altitude, owing to the corresponding drop in the magnetic field, and the data provide information on the electron energy spectrum as a function of position, and therefore clues on where the electrons are accelerated. Chen also described how the wide bandwidths provided by EOVSA enable a new kind of study of sunspots; since the frequency of the emission observed is proportional to the harmonic number times the gyrofrequency, which is in turn a function of the magnetic field, it is possible to effectively map the magnetic field in 3D.

Another key instrument for solar work in recent years is the upgraded VLA, which has been available for solar observing in the 1–8 GHz range since 2011 (with plans underway to commission additional higher and lower frequency bands). The VLA can provide time and frequency resolution of up to 5 ms and 1 MHz, respectively, with up to ~10 k channels, implying that it is, in theory, possible to create millions of images per minute of observation. Chen highlighted several recent results from VLA solar observations.

A longstanding puzzle has been the mechanism responsible for the conversion of magnetic energy into the kinetic energy required for the acceleration of relativistic particles during solar flares. A leading candidate has been termination shocks, which can occur when a high-speed jet speed exceeds the local Alfvén speed. Such shocks are predicted by numerical simulations, but their existence had yet to be convincingly established observationally. As described by Chen, this has changed thanks to recent high-cadence imaging spectroscopy of a solar flare with the VLA, in combination with UV and X-ray observations (Chen et al. 2015). With the VLA, Chen's team found short-lived bursts of radio emission coincident with the predicted location of the termination shock. Density fluctuations along such a termination shock map to different frequencies, so by taking a dynamic spectrum it becomes possible to map the evolution of the shock surface. The VLA dynamic spectra revealed that upon arrival of the reconnection outflow, the shock fragmented. In tandem, hard X-ray data showed that the electron energy distribution became softer. Thus, Chen et al. concluded that the termination shock must be at least partially responsible for electron acceleration in the flare.

Another topic addressed by Chen is the recent use of the VLA to trace fast electron beams associated with type III solar bursts. Electron beams travel up and down along magnetic field lines, encountering different densities along the way, resulting in corresponding changes in the frequency of the emitted radio waves. With the ability to make images at multiple frequencies within a dynamic spectrum, it becomes possible to map the electron trajectories in the solar corona. New data obtained by Chen and collaborators show that during a type III burst, all of the electron beams originate from a single point in the corona believed be the reconnection site. In these types of events, it therefore appears that the reconnection event is responsible for accelerating electrons.

Finally, while bremsstrahlung and gyromagnetic radiation dominate the solar emission at cm wavelengths, ECM emission can also operate at these frequencies and is believed to have powered a 2006 spike burst event whose strength (10^{10} Jy over 1–2 GHz) was sufficient to knock out global positioning systems (Gary et al. 2007). The implications of such events are clearly important to Earth, but as S. White pointed out, the origin of this emission is is still not well understood and the auroral model for ECM that works for chemically peculiar stars and UCDs (Section 6) cannot be applied.

8.3. The Sun at Millimeter Wavelengths

Solar observing with ALMA using its Band 3 (100 GHz) and 6 (230 GHz) receivers became possible for the first time in late 2016 (e.g., White et al. 2017). ALMA is now able to probe the solar chromosphere on scales from ~1–1.003 $R_\odot$ with unprecedented sub-arcsecond angular resolution, providing data free from the complications of the non-LTE effects that impact traditional UV emission line studies. Commissioning of additional ALMA bands for solar work, as well solar polarization capabilities, remains ongoing.

Because ALMA's solar capability is so new, many of the first data are still being analyzed, but RS-2 participants saw

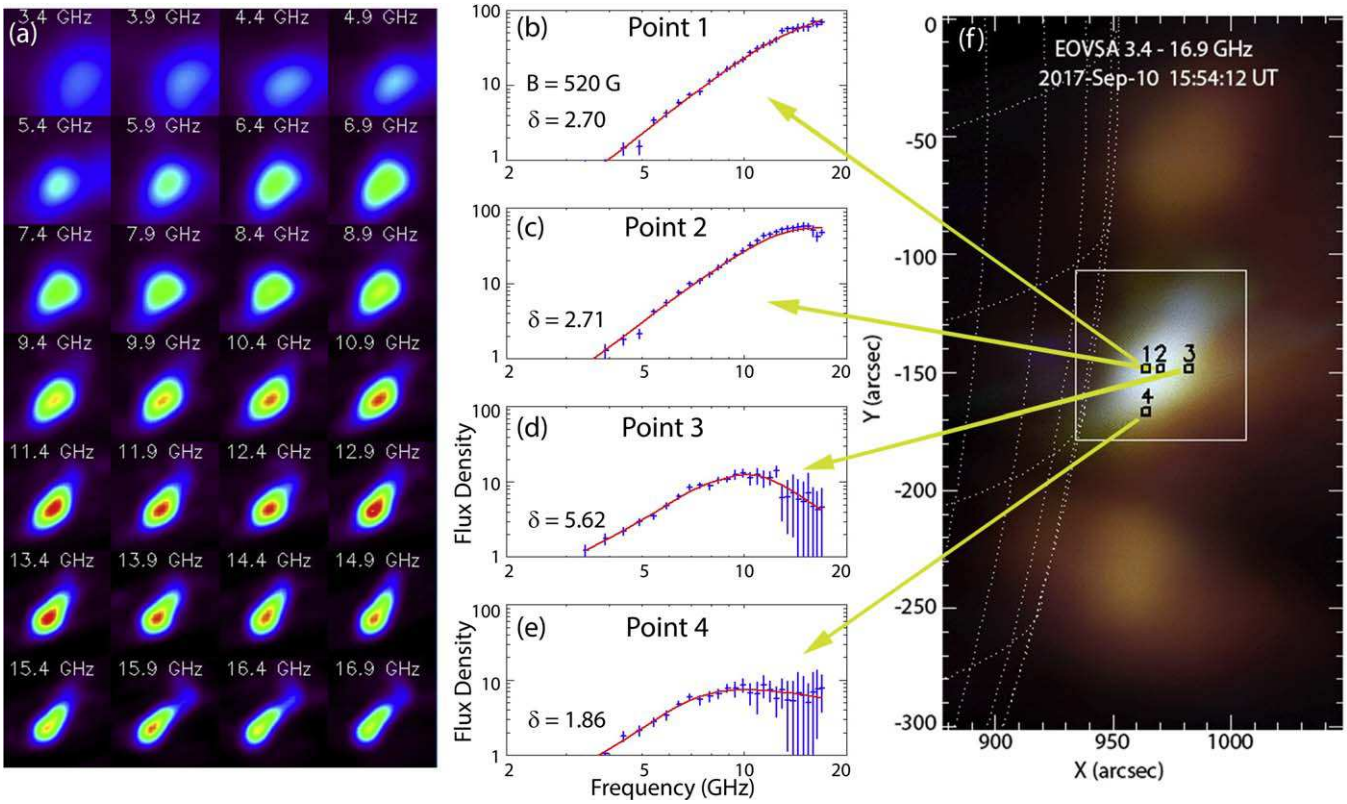

Figure 3. Single-frequency images and spatially resolved gyrosynchrotron spectra of a solar limb flare observed with the EOVSA on 2017 September 10. The field of view of each image corresponds to the white box in the right-hand panel. The spectra are extracted from single image pixels and have a scale in solar flux units per pixel, where the pixel area is $2'' \times 2''$. Reproduced from Gary et al. (2018). © AAS.
(A color version of this figure is available in the online journal.)

some exciting previews. For example, B. Chen showed how images of sunspot oscillations obtained with ALMA can be compared with those at other wavelengths (extreme UV, Hα) to constrain the height where the oscillation is occurring. J. Linsky and S. White also briefly touched on the potential of ALMA for measuring chromospheric magnetic fields via circular polarization measurements (see also Section 5.2). However, such work will be challenging, as theoretical work by White and collaborators found that the expected degree of predicted polarization in the quiet Sun (excluding sunspots) is quite small ($\lesssim$1%; Loukitcheva et al. 2017).

9. Stellar Winds across the H-R Diagram

K. Gayley began his review of stellar winds with the observation that it is far easier to explain why stars should not have winds than it is to explain why they do. He clarified by pointing out that powering a wind requires moving heat from the stellar interior to its surface and, in general, the ratio of the surface temperature to the interior temperature will be too small to allow escape of material from the surface (e.g., a dwarf will typically have $\sim 10^{-3}$ times the energy at the surface needed for escape). One way to overcome this is to deposit heat onto the surface in places where the density is low, raising the outside temperature to a level comparable to the inside temperature, and consequently pushing the thermal velocity to close to the escape velocity. Another option is to mechanically push the surface out. This can be achieved with radiation pressure on dust (as in cool asymptotic giant branch (AGB) stars; Section 11.3) or line opacity (as occurs for high-luminosity stars; Section 10.1); magnetohydrodynamic waves or field stresses (for rapid rotators; e.g., Section 10.1.4); or through gas pressure heated by waves or reconnection events (as in coronal-type winds; Section 5.1).

Gayley pointed out that in dwarfs (Section 5.1), coronal winds must overcome enormous and efficient radiative line cooling that become increasingly important as temperatures approach $\sim$100,000 K (or equivalently, $v_{\rm esc} \sim 40\,{\rm km\ s^{-1}}$). Getting over this radiative cooling "barrier" necessitates having very low-density gas, implying that it is not possible to have a high-density coronal wind. On the other hand, in giants, where the escape velocity is lower, achieving a high thermal speed is no longer necessary ($T \sim$ 20,000 K), and somewhat denser "chromospheric winds" can be achieved. Gayley proposed that

this distinction likely accounts for the so-called "coronal graveyard"[4] first identified by Linsky & Haisch (1979), although more work is needed (see also Suzuki 2007). He also suggested that this type of driving mechanism may be responsible for the "superwinds" of AGB (Section 11.3) or red supergiant (RSG) stars (Section 12.3), although additional radiative driving would probably be required to power these fast, dense winds. For high-luminosity stars, radiation pressure can drive winds, given a source of opacity in the form of dust [as in AGB stars (Section 11.3) and possibly RSGs (Section 12.3)], continuum radiation (as in luminous blue variables), or UV resonance lines (as in Wolf-Rayet (W-R) stars, blue supergiants, main-sequence OB stars (Section 10.1), and the central stars of planetary nebulae (PNe; Section 14.2).

Gayley concluded by listing several unsolved problems concerning stellar winds where radio observations are likely to provide new insights. These included

(1) How is mass loss affected by rapid rotation or strong magnetic fields? While rotation helps to remove some of the gravitational barrier, it does not increase mass loss at the equator. Instead, the star will tend to bulge at the equator (become oblate), causing the radiative flux to emerge from the poles. An exception is if the star is spun up to critical rotation, in which case a disk will form that is unrelated to the wind (as in the Be stars; Section 10.2).

(2) How can we gauge the past and future properties of winds? Are they continuous or episodic? Do they increase or decrease with age? Gayley noted that 21 cm line observations of AGB stars (Section 11.3) are of interest in this regard, since they probe the entire history of the mass loss, including distances beyond which traditionally used molecular tracers of the circumstellar material become dissociated by the interstellar radiation field. In addition, the presence of knots and other features in the H I gas provide clues on whether the mass loss is episodic (see Matthews et al. 2013).

10. Radio Emission from Hot Stars

10.1. Hot Star Winds

The most massive stars have strong winds that produce significant rates of mass loss ($\sim 10^{-6} - 10^{-4}\, M_{\odot}\, \mathrm{yr}^{-1}$), with important consequences for the evolution of the star and for the surrounding interstellar medium (ISM). The basics of hot star winds are now relatively well understood. These winds are radiatively driven, with line absorption providing the dominant opacity, and are typically described by the so-called "CAK" theory (Castor et al. 1975). However, some important questions remain, and the review talks by I. Stevens (University of Birmingham) and K. Gayley touched on how radio observations can be uniquely exploited in the quest to answer them.

Radio emission mechanisms that are relevant for studying the winds of massive stars include thermal free–free emission from the ionized winds of single stars and the nonthermal (synchrotron) emission that can arise from colliding winds in binaries (Section 10.1.2). Other possible, though less explored radio emission mechanisms include magnetic reconnection events in interacting binaries (leading to particle acceleration) and ECM emission (see Section 10.1.4), but with different plasma conditions compared to the low-mass star case (cf. Section 6). The winds of runaway massive stars can also impact the ambient medium, creating a bow shock that emits both thermal and nonthermal radio emission (Benaglia et al. 2010; Brookes et al. 2016a).

The winds of massive stars are dynamically unstable, as the radiative driving is very non-linear, leading to shock formation and clumping. Because free–free emission depends on the density squared, clumping will enhance the radio emission and produce variations in the spectral index as a function of frequency (e.g., Daley-Yates et al. 2016). Radio observations therefore provide unique insights into the nature of this clumping (Section 10.1.1). Compared with X-ray and Hα emission in massive star winds, which arise from within a few stellar radii, different radio wavelengths also have the advantage that they are able to probe from tens of stellar radii (submm) to hundreds of stellar radii (1 GHz).

While there is general agreement that radio observations supply one of the best means of deriving mass-loss rates for hot stars (relying on fewer assumptions than other methods), Gayley emphasized that current factors of 2–3 uncertainty in typical $\dot{M}$ values can have important consequences for the impact of the mass loss on the evolution of a given star. Further refinement of these values through better observations and modeling therefore remains important.

Stevens noted that higher radio frequencies (mm/submm) begin to probe the little-understood acceleration regions of hot star winds. He pointed out that the effect of seeing into the acceleration region of the wind at these wavelengths can produce a flux excess compared with a canonical Wright & Barlow (1975) model, leading to a non-linear spectral index and causing errors in derived mass-loss rates if not accounted for (Daley-Yates et al. 2016). The effects of clumping (in particular, radius-dependent clumping; see also below) can further complicate interpretation of the mm/submm part of the spectrum, leading to degeneracies in wind models between the velocity law and the amount of clumping. An additional effect may be produced by He recombination in different regions of the wind, leading to more electrons than expected in the inner wind compared with the outer wind. Stevens noted that the acquisition of continuous radio spectrum over three orders of magnitude in frequency might be able to disentangle these various effects, but we presently lack such data, and indeed, most hot star radio "spectra" contain just a few points.

[4] The term "coronal graveyard" has been used to mark the dividing line beyond which giants are not found to display coronal signatures in the X-ray and UV; in general, coronae are not seen in giants redward of spectral type K1 III (Ayres 2018 and references therein).

10.1.1. The Effects of Clumping

R. Ignace (East Tennessee State University) discussed clumping and other effects that must be properly treated to accurately interpret radio observations of the ionized winds of hot stars. He noted that with "microclumping" (effectively a modified smooth wind), the clumps are optically thin, hence their shape is unimportant. However, this type of clumping affects the observed radio flux density and must be accounted for to accurately derive mass-loss rates; ignoring the clumping leads to overestimates of $\dot{M}$.

In the case of "macroclumping," the wind is composed of discrete density structures with a range of optical depths. The resulting effects have been previously studied in the X-ray and UV, but little explored until now in the radio bands (Ignace 2016). Ignace showed that because the clumps are optically thick, different clump geometries can in principle be expected to have observable effects on both the radio fluxes and the slope of the SED. However, in two sample geometries that he considered—fragments ("pancakes") and spheres—the effects are not significantly different from the microclumping case, except when the spherical clumps have a very substantial volume-filling factor.

Ignace also revisited the earlier work of White (1985) that reported evidence of synchrotron emission from apparently single OB stars. Some preliminary model calculations performed by Ignace raise the question of whether the presence of synchrotron emission might in some cases be misinterpreted as wind clumping gradients (e.g., in the case of ζ Pup; cf. Ignace 2016).

10.1.2. Colliding Wind Binaries

In close massive binaries, wind interactions can produce shock regions that are believed to be sites of particle acceleration and the production of nonthermal radio emission (De Becker & Raucq 2013; De Becker et al. 2017). However, there are some close OB binaries with no such radio emission. I. Stevens suggested that one possible explanation is that the emission is dependent on the degree of magnetic field alignment.

As described by Stevens, low-frequency (meter wave) observations are useful for identifying the turnover frequency for colliding wind binaries, and he described such observations recently undertaken for one such binary, WR 147, using the GMRT at 235 and 610 MHz. The system was undetected at 235 MHz, indicating a steep downturn in the SED at low frequencies. A lingering puzzle is that the nonthermal emission defies fitting using a simple model comprising synchrotron plus free-free absorption (Brookes et al. 2016b). Clumping may play a role, but more data points along the radio spectrum are needed to distinguish between possible explanations.

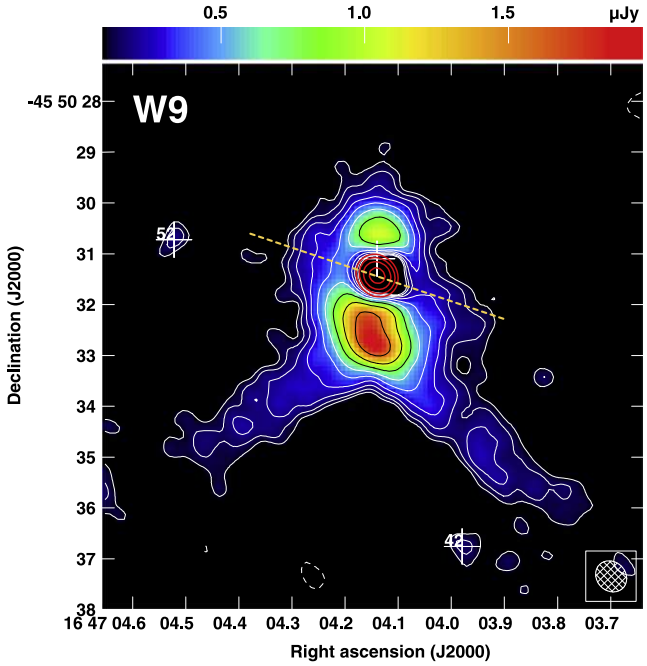

Figure 4. ALMA 100 GHz image (contours and color scale) of the sgB[e] star Wd1-9, a member of the 5-Myr-old cluster Wd1. The extended emission contours (white) are $(-1,\ 1,\ 1.4...16) \times 99\ \mu$Jy beam^{-1}; for the compact source (red) they are $(0.1,\ 0.14,\ 0.2,\ 0.28) \times 416$ mJy beam^{-1}. The dashed line indicates the orientation of an apparent bipolar outflow. Wd1-9 exhibits similarities to the enigmatic radio star MWC 349A (Section 12.2). From Fenech et al. (2018) reproduced with permission. © ESO.
(A color version of this figure is available in the online journal.)

10.1.3. Massive Stars in Clusters

Work presented by D. Fenech (University College London) highlighted the unique power of ALMA for studying the mass-loss properties of massive stars and their interactions with their environments. She presented results from a comprehensive analysis of the full Westerlund 1 (Wd1) cluster based on 3 mm ALMA data (Figure 4). Her team identified 50 radio-emitting stars within this 5 Myr-old cluster, spanning a wide range of stages of post-main-sequence evolution for massive stars, including 21 W-R stars and a number of cool and warm supergiants/hypergiants. They used the mm data to derive mass-loss rates for the sample (Fenech et al. 2018). Unexpectedly, they also uncovered emission nebulae surrounding a number of OB and W-R stars in Wd1, which they suggest result from the interaction between the stellar ejecta and the intracluster medium. The presence or absence of such a nebula around a massive star of a given type is expected to have important implications during the subsequent supernova explosions of these stars, as it may affect the light curve, spectrum, and other phenomenology of the evolving ejecta. Another surprise was that more than half of the stars appear to be spatially resolved. It is unlikely that the observations are resolving the stellar winds; the

inferred sizes are ∼20–100 times the expected size of the radio photospheres (which are predicted to range from ∼0.1 to 3.8 mas; Fenech et al. 2018), and the presence of dust around these hot stars also seems unlikely. The explanation for this finding is therefore unclear, but it may be related to the interaction between the winds and the cluster environment.

Observations of Wd1 were also performed recently using the Australian Telescope Compact Array (ATCA) at 5.5 and 9 GHz by H. Andrews (University College London) and collaborators. Andrews presented preliminary results on some of the discovered radio sources. The observations uncovered evidence for asymmetric ejecta surrounding 3 M-type supergiants and three cool hypergiants in the cluster. These detections provide the first ever evidence of cometary-like nebulae associated with yellow hypergiants (Andrews et al. 2018). The alignment of the observed asymmetries relative to the cluster center shows clear evidence of a cluster outflow. F. Yusef-Zadeh noted that a similar phenomenon has also been seen for stars near the Galactic center.

A second presentation by Fenech reported on the "COBRaS" project (Morford et al. 2017), a survey of the core of the young massive cluster Cyg OB2 at 1.6 and 5 GHz using the optical fiber-linked Multi-Element Radio Linked Interferometer Network (e-MERLIN). When completed, the survey will comprise ∼300 hours of observations spanning multiple pointings and covering approximately 20 arcmin^2. Importantly, the combination of μJy sensitivity and excellent angular resolution (∼40 mas at 5 GHz) will suppress contamination from diffuse emission and enable the detection of free–free emission from the winds of individual massive stars, allowing the determination of mass-loss rates. The 1.6 GHz observations have now been completed (Morford et al. 2016) and one surprising finding is that the only non-binary massive stars detected are the luminous blue variables. To date, about half of the identified radio sources show no counterparts at other wavelengths. Robust upper limits on mass-loss rates were obtained for a number of OB giants and supergiants that in turn provide useful constraints on the wind geometry and clumping. Four transients have also been identified in this sample.

10.1.4. Magnetic OB Stars

Another class of hot star that emits nonthermal radio emission is the rapidly rotating Magnetic Chemically Peculiar (MCP) stars. Stevens highlighted recent work on the MCP star CU Vir where two radio peaks per rotation period are seen, both with 100% circular polarization. Trigilio et al. (2011) attribute this to magnetospheric ECM emission. However, there is a discrepancy between the optical and radio light curves of this star that is not understood. Stevens stressed the importance of multi-frequency radio studies of other MCP stars across their entire rotation period (including high-frequency observations that will permit peering deeper into the magnetospheres) to determine whether CU Vir is unique.

10.2. Be Star Disks

Classical Be stars are surrounded with self-ejected, rotationally supported, slowly outflowing gaseous disks that are ionized by the hot, rapidly rotating central star. The disk physics are dominated by viscous processes, which provide the outward transfer of angular momentum. Because the disks are ionized and emit free–free emission, the cool outer regions can be uniquely probed by cm-wave observations. Radio observations can then be combined with data at other wavelengths (extending shortward to the UV) that sample the inner disk and the star itself to provide important tests of models.

As described in the presentation by R. Klement (Center for High Angular Resolution Astronomy, Georgia State Univ.), the inner parts of Be disks ($r \lesssim R_\star$) appear to be well explained by the so-called viscous decretion disk model (Lee et al. 1991), but relatively little is known about the outer parts of the disks, including the effects that may be produced by a binary companion, and the location of the critical radius (transonic boundary). The latter marks the point where the radial velocity exceeds the sound speed and viscosity can no longer transport angular momentum, leading to disk dissipation.

Until recently, only eight Be stars had been detected at radio wavelengths (Waters et al. 1991; Dougherty & Taylor 1992), but Klement described the results of a recent study of six Be stars using new and archival radio observations in combination with multiwavelength data and radiative transfer modeling (Klement et al. 2017). Klement et al. found that in all cases, the cm-wavelength flux densities lie below the predictions of non-truncated disk models. But at the same time, the SED shapes rule out a sharp disk truncation. This suggests the presence of disk material beyond the truncation radius, and a plausible explanation is that all of these stars are binaries with circumbinary disks. Indeed, binarity is already confirmed for two of the stars. One of these is β CMi, where the companion search was motivated by the radio results (Dulaney et al. 2017). Work is ongoing by Klement and collaborators to study additional Be stars at cm and mm wavelengths.

11. AGB Stars

For stars with initial masses in the range 0.8–8.0 $M_\odot$, xthe AGB marks the second ascent of the red giant branch, at which point post-He burning stars reach luminosities of up to $\sim 10^4\ L_\odot$, and their temperatures cool to 2000–3000 K. These cool temperatures are conducive to dust and molecule formation, and a key property of AGB stars is their intense stellar winds ($\dot{M} \sim 10^{-8}$ to $10^{-4}\ M_\odot\ \mathrm{yr}^{-1}$), which contribute significantly to the dust and heavy element enrichment of the ISM (see Höfner & Olofsson 2018). The continuing importance of radio

wavelength observations for understanding AGB stars was reviewed by H. Olofsson (Chalmers University).

11.1. Radio Photospheres

The imaging of the radio photospheres of AGB stars was pioneered by Reid & Menten (1997). Olofsson drew attention to recent developments on this topic, including the improved ability of current-generation radio interferometers to resolve details on the surfaces of nearby AGB stars (Matthews et al. 2015, 2018; Vlemmings et al. 2017), and the possibility to perform comparisons of these results with the predictions of state-of-the-art 3D models, which now include convection, pulsation, and dust condensation (Freytag et al. 2017).

Radio photospheres lie above the optical photosphere, but inside the dust-condensation radius, making them an excellent probe of shocks and thermal structure within the regions of the AGB star atmosphere where the stellar wind is accelerated and launched. Because of the frequency-dependence of the free–free opacity, different radio frequencies are expected to probe different depths in the atmosphere (Reid & Menten 1997); this has now been confirmed observationally in one AGB star (Matthews et al. 2015) and one RSG (Lim et al. 1998; O'Gorman et al. 2015).

The wide bandwidths available with the VLA and ALMA now permit the simultaneous imaging of molecular lines along with the radio photosphere, and these lines can be used as kinematic probes of the atmosphere. One example is the recent work of Olofsson and his collaborators that used ALMA to image W Hya in the 338 GHz continuum, as well as in the CO $v = 1, J = 3 - 2$ line (Vlemmings et al. 2017). These authors reported evidence for a "hot spot" with $T_B > 5 \times 10^4$ K that they interpreted as a chromosphere with a low volume-filling factor. Against the stellar disk, the aforementioned CO line is seen in both emission and absorption due to the presence of infalling and outflowing gas, suggestive of both cool ($T \approx 900$ K) and warm ($T \approx 2900$ K) molecular layers and the presence of shocks with velocities $\sim$20 km s^{-1}. However, Olofsson emphasized that current models cannot fully explain these results, hence follow-up, including additional epochs of observations and observations of additional stars, are needed.

11.2. Circumstellar Masers in AGB Stars

L. Sjouwerman (NRAO) described results from the analysis of a large sample of SiO maser-emitting evolved stars that have been observed as part of the Bulge Asymmetries an Dynamical Evolution (BAaDE) project (Trapp et al. 2018; Section 16). An important piece of this project is the characterization of how biases and selection effects may impact the results. As described by Sjouwerman, such investigations also have interesting implications for understanding the underlying stellar astrophysics. As part of this effort, his team collected near-simultaneous (same-day) measurements of the both 43 GHz and 86 GHz SiO $\nu = 1$ maser lines for nearly 100 stars using the ATCA (Stroh et al. 2018). A systematic comparison of the line parameters for the two transitions revealed that the mean flux density ratio is consistent with unity. They also found that the 43 GHz transition gets successively weaker in AGB stars with thinner circumstellar envelopes (CSEs). But in contrast to both theoretical predictions (Humphreys et al. 2002) and previous empirical findings based on smaller samples (e.g., Pardo et al. 1998), they find no evidence for a turnover in the NIR colors of Mira-type CSEs beyond which the 86 GHz line is consistently brighter. This has implications for the pumping mechanism of the masers and the physical conditions under which the respective transitions can arise.

11.3. Mass Loss from AGB Stars

Olofsson underscored that understanding AGB mass loss is fundamental to understanding AGB stars, as their evolutionary tracks are strongly dependent on how much mass these stars lose at various times along the AGB. However, this is a highly complex problem, since mass loss depends on many stellar parameters, including mass, luminosity, temperature, and metallicity, all of which evolve with time. Indeed, Olofsson pointed to understanding the temporal evolution of AGB mass loss as a key unsolved problem.

Current evidence points to increasing mass-loss rates toward the end of the AGB, leading up to a superwind phase. Initial-final mass relations (e.g., Cummings et al. 2016) necessitate that stars lose up to 80% of their initial mass on the AGB, but the cause of the superwind remains unknown, and observations paint a confusing picture of the stages leading up to it. Olofsson drew attention to the puzzling findings of Justtanont et al. (2013), who looked at a sample of extreme OH/IR stars thought to be in the very late stages of the evolution on the AGB. Based on a dynamical model, these authors inferred mass-loss rates as high as $\dot{M} \approx (2 - 10) \times 10^{-4}\, M_\odot\, \mathrm{yr}^{-1}$. However, values inferred from observations of low-J CO lines are far lower ($\approx 3 \times 10^{-6}\, M_\odot\, \mathrm{yr}^{-1}$). A further conclusion is that the superwind phase lasts only 200–600 years, which is too short to produce the required amount of mass loss. One possibility is that there are several superwind phases, and Olofsson proposed searching for possible signatures by using ALMA to map out the distribution of multiple CO lines.

A prescription for mass-loss rate based on stellar parameters is also an important ingredient for modeling the stellar populations and chemical yields in galaxies, including the contributions of AGB stars to integrated galactic light, dust production, and element synthesis. Currently the best mass-loss rate prescription we have is the one based on pulsation period (Vassiliadis & Wood (1993); Figure 19 of Höfner & Olofsson 2018). Indeed, A. Zijlstra noted that the very existence of a correlation between period and $\dot{M}$ may indicate that pulsation is the primary driver of mass loss during much of

the AGB. However, Olofsson stressed that there has been little progress on this topic for nearly 30 years. He proposed attempting to observe AGB stars during some well-defined process (e.g., a thermal pulse) and assess how that affects the mass-loss rate (e.g., Kerschbaum et al. 2017).

To explore the effects of metallicity on mass loss, it is crucial to expand the observations of AGB stars beyond the Milky Way. This has now become possible with ALMA, and Olofsson was part of a team that recently obtained CO detections of four carbon stars in the Large Magellanic Cloud (Groenewegen et al. 2016). However, Olofsson noted that even with ALMA, it will likely be difficult to perform such observations beyond the Magellanic Clouds.

Olofsson provided a reminder that the H I 21 cm line can serve as a valuable tracer of the atomic component of the circumstellar environments of AGB stars, particularly for warmer AGB stars. The weakness of the circumstellar H I line, coupled with the ubiquity of strong interstellar H I emission along the line of sight make such observations challenging, but the number of AGB stars surveyed in the H I line has grown to well over 100 (Gérard & Le Bertre 2006; Gérard et al. 2011 and in preparation; Matthews et al. 2013). Detection rates are high for irregular and semi-regular variables with moderate mass-loss rates ($\lesssim 10^{-7}\,M_{\odot}\,\mathrm{yr}^{-1}$), but detections of Mira variables and higher mass-loss-rate stars are rare. Modeling by Hoai et al. (2015) has shown that this cannot be readily attributed to radiation transfer effects, and most likely implies that the circumstellar material in these cases is largely molecular.

A program to study the CSE of an AGB star in "3D" was described by M. Guélin (Institut de Radioastronomie Millimétrique; hereafter IRAM). His team recently used a combination of the Submillimeter Array (SMA), the IRAM 30 m telescope, and ALMA to study the CSE of the nearby carbon star IRC+10216 in a variety of molecular lines and with various spatial resolutions. They then used the combined results to constrain 3D models of the CSE velocity structure, in addition to characterizing the star's mass-loss history and the physical conditions of the CSE a function of radius (Guélin et al. 2018). IRC+10216 is well known to have a massive, dusty envelope with a relatively symmetric shape, albeit with considerable fine structure. The new observations of Guélin et al. show a quasi-regular pattern of multiple thin rings of various radii within the CSE, as traced by molecules such as CO(2-1) (Figure 5). Although roughly centered on the star, these various rings are not concentric. However, Guélin's team has shown that these features are true shells (not part of a spiral pattern), with densities that are ∼3× higher than the inter-shell regions. In the outer envelope, the shell spacing of ∼16″ (∼2000 AU) corresponds to timescales of ∼700 yr, while in the inner CSE ($r < 40''$) the shell spacing is smaller. Guélin's team has proposed that these properties of the IRC+10216 CSE are the result of mass loss modulated by a low-mass companion with an orbit in the plane of the sky. They also examined the question of whether the mass loss from IRC+10216 is isotropic by applying newly developed algorithms to reconstruct their 3D position–velocity data. Based on the results of this analysis they concluded that IRC+10216's shells are spherical in shape, hence the mass loss is isotropic (or nearly so).

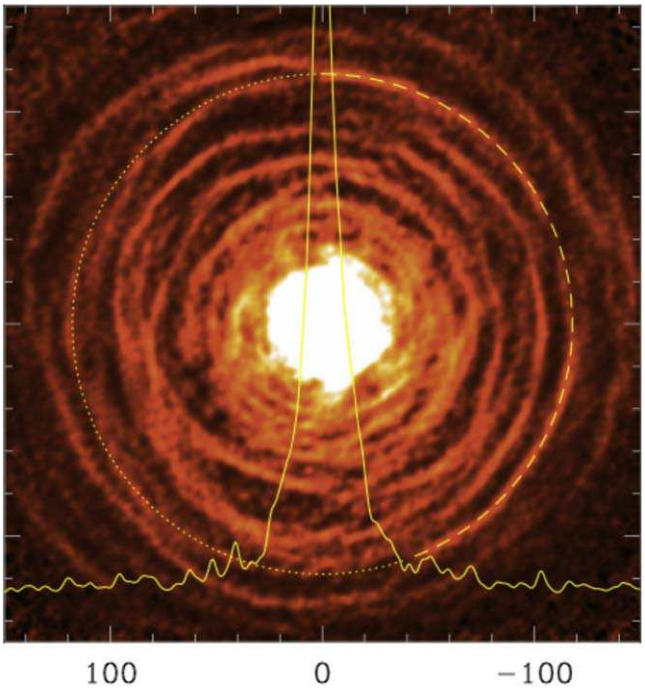

Figure 5. Circumstellar CO(2−1) emission at the stellar systemic velocity (−26.5 km s^{-1}) surrounding the AGB star IRC+10216. The map combines interferometric data from the SMA and short-spacing data from the IRAM 30 m telescope. The scale is in arcseconds. The yellow line shows an intensity profile along an east-west strip through the stellar position. From Guélin et al. (2018), reproduced with permission. © ESO.
(A color version of this figure is available in the online journal.)

11.4. Circumstellar Chemistry

H. Olofsson noted that ∼90 molecules have now been detected in the CSEs of AGB stars, but numerous unidentified lines are also present in the mm and submm bands. He emphasized the importance of unbiased wideband spectral scans with single-dish telescopes for the discovery of additional circumstellar species and for advancing our understanding circumstellar chemistry (e.g., Cernicharo et al. 2000; Zhang et al. 2009; Chau et al. 2012; Velilla Prieto et al. 2017; De Beck & Olofsson 2018). As the number of such studies has recently grown, it has become possible not only to compare in detail C- and O-rich stars, but also to discern more subtle differences among individual stars of the same chemistry.

Single-dish studies are a crucial complement to interferometric imaging, since the latter often resolves out a significant

fraction of the flux in circumstellar lines (e.g., Cernicharo et al. 2013). Further, with today's wide bandwidth systems, Olofsson pointed out that data from single-dish telescopes can serve another vital role in situations where multiple transitions of a given molecule with very different energy requirements can be observed and interpreted in concert (e.g., Van de Sande et al. 2018); in this case, excitation energy rather than spatial resolution can serve as a radial discriminator. When used in conjunction with radiative transfer models, such data help in understanding the dynamical and chemical structure of AGB winds.

Isotope ratios are very important tracers of stellar nucleosynthesis, and as an example, the $^{12}C/^{13}C$ ratio in the ISM is believed to be predominantly set by AGB stars. It therefore serves as a marker of the stellar mass function and star formation history. Ramstedt & Olofsson (2014) recently undertook a comprehensive analysis of this ratio for a large sample of AGB stars and found that while it varies for the three different chemical types (M, S, and C), it is surprisingly independent of mass-loss rate. Interestingly, their results also suggest that PNe (see also Section 14.2) are preferentially drawn from stars with low $^{12}C/^{13}C$. Another isotope ratio of interest is $^{17}O/^{18}O$, which is set during the red giant branch and does not evolve during the AGB. Olofsson and his colleagues have shown that this ratio can serve as an initial mass estimator for stars with $M_\star \lesssim 4\,M_\odot$ (de Nutte et al. 2017). Their work also underscored an important limit of $M_\star \lesssim 1.5\,M_\odot$ below which carbon stars do not form.

11.5. Disks around AGB Stars

The longstanding question of how nearly spherical AGB stars evolve into the complex morphological varieties of PNe is still not fully solved (see also Section 14.2). However, the formation of disks owing to the influence of a binary companion is suspected of playing a key role. L_2 Pup now represents the first example of a disk being directly detected around a bona fide AGB star (Lykou et al. 2015; Kervella et al. 2016; Homan et al. 2017). As described by Olofsson, high-resolution ($\sim$15 mas) observations of SiO lines using ALMA reveal that at least a portion of the disk appears to be in Keplerian rotation, implying a mass for the central star of $0.66\,M_\odot$. The estimated initial mass is $\sim 1\,M_\odot$, implying that L_2 Pup is a solar-like star that has lost $\sim$40% of its mass (Kervella et al. 2016). In addition, the ALMA data reveal evidence of a companion visible in both the continuum and the CO(3-2) line. Its estimated mass ($\sim 12\,M_J$) lies at the border between brown dwarfs and planets. However, as pointed out by A. Zijlstra, such a low mass for the companion makes it difficult to account for the disk's angular momentum.

11.6. Magnetic Field Measurements of AGB Stars

Olofsson reminded us that it has been notoriously difficult to determine the properties of magnetic fields associated with AGB stars, but this is of critical importance for better understanding the role of B-fields in determining the mass-loss characteristics of stars during the AGB and post-AGB phases. He pointed to the enormous potential that radio interferometry has to contribute to this topic through polarization studies of both thermal and maser lines, including measurements of the Zeeman effect in species such as SiO, H_2O, OH, and CN and the Goldreich-Kylafis effect in CO and other lines. Olofsson pointed out that to date, there is only one measurement of a magnetic field on an AGB star (the S-type star χ Cyg; Lèbre et al. 2014); in all other case the circumstellar magnetic field is extrapolated inwards (e.g., Booth et al. 2012; Duthu et al. 2017).

12. Radio Emission from Supergiants

12.1. Cepheids

Studies of Cepheid variables provide crucial insights into the evolution of intermediate mass stars, and understanding their physics is also of significant interest given their longstanding role in establishing the extragalactic distance scale. Cepheids have received relatively little attention at radio wavelengths, and with the exception of two Cepheids that appear to be associated with 21 cm line-emitting circumstellar nebulae (Matthews et al. 2012, 2016), no radio detections of Cepheid have ever been reported (Welch & Duric 1988; L. Matthews et al. 2018, in preparation). However, recent work by N. Evans (CfA) and collaborators provides a new motivation for re-examining these stars in the radio. Using *Chandra* and *X-Ray Multi-Mirror Mission (XMM-Newton)* observations of Cepheids, they have discovered surprising bursts of X-rays at a pulsation phase just after maximum radius (Engle et al. 2014, 2017; Evans et al. 2016). One possible explanation is that these bursts are caused by shocks related to the pulsation process; another is that they are a flare-like phenomenon triggered by the collapse of the atmosphere. Evans noted that detections of a radio counterpart to these events could provide additional clues on their origins. The predicted radio flux densities are highly uncertain, but present estimates suggest they are likely to be detectable with the VLA during particular phases of the pulsation cycle. Discovery of this phenomena is intriguing in light of the longstanding question of whether Cepheids are undergoing significant pulsationally driven mass loss (e.g., Neilson 2014).

12.2. The Enigmatic Radio Star MWC 349A

V. Strelnitski (Maria Mitchell Observatory; MMO) described recent work on the brightest stellar radio continuum source in the Galaxy, MWC 349A. MWC 349A is surrounded

by a dense H II region, and to date is the only star known to exhibit high-gain atomic maser and laser emission in H RRLs. These masers appear to trace a disk and photoevaporating wind (Zhang et al. 2017). MMO has monitored MWC 349A in the optical (*VRI*, Hα) and radio (maser lines) for over 20 years, amassing a unique data set on this star (Thomashow et al. 2018).

MWC 349A appears to be a massive object ($>10\,M_{\odot}$), but its evolutionary status has remained a matter of dispute. Indeed, part of the problem, as noted by Strelnitski, is that evolution from the PMS to an evolved (supergiant) star spans only $\sim$5 Myr for stars of this mass. Gvaramadze & Menten (2012) argued that MWC 349A is an evolved massive star (luminous blue variable) based on its photometric and spectroscopic variability, as well as evidence for the probable ejection of MWC 349A and the neighboring B0III star MWC 349B from the Cyg OB2 association several Myr earlier. However, new results from Strelnitski and collaborators (Drew et al. 2017) find a radial velocity difference of $\sim$35 km s^{-1} between MWC 349A and MWC 349B, indicating that they are unlikely to have been bound. Based on this, along with evidence of a possible physical association between MWC 349A and a compact molecular cloud (Strelnitski et al. 2013), Strelnitski argued that MWC 349A may instead be a YSO.

D. Fenech disputed the latter conclusion, pointing to recent ALMA observations of the B[e] supergiant Wd1-9 that show mm properties extremely similar to MWC 349A (Fenech et al. 2017, 2018; Figure 4; see also Section 10.1.3). Fenech therefore argued that the latter too is likely to be an evolved star. However, one difference noted by I. Stevens is that the RRL profiles of Wd1-9 are Gaussian-like (Fenech et al. 2017), in contrast to the double-peaked lines seen in MWC 349A (e.g., Báez-Rubio et al. 2013). M. Reid went further to offer the provocative suggestion that MWC 349A might be a pre-planetary nebula. Ultimately no consensus was reached at the meeting regarding the evolutionary status of this object.

12.3. Red Supergiants

A. Richards described some recent advances in the study of RSG winds and outflows based on the detailed analysis of circumstellar masers. A wide variety of mm/submm maser transitions lie within bands accessible with ALMA, spanning a considerable range of excitation conditions. When observed in combination at high spatial resolution, these lines supply powerful constraints on the physical conditions (density, temperature) and kinematics over a wide range of radii within the extended atmospheres of cool evolved stars (see Gray et al. 2016). Importantly, such information can supply constraints on models for the shaping and acceleration of RSG winds.

As an illustration, Richards presented recent results for several mm/submm H_2O transitions observed with ALMA toward VY CMa (Richards et al. 2014). Richards's team found that the 183 GHz H_2O masers are far more extended than any other previously observed H_2O transitions and appear to follow the distribution of the extended, dust-scattered light seen in *Hubble Space Telescope* images (Humphreys et al. 2007), implying a link with small, cool dust grains and low-density gas (Richards et al. 2018). Other high-frequency H_2O maser transitions at 325, 321, and 658 GHz were seen to lie in thick, irregular shells and trace, respectively, material progressively closer to the central star. The surprisingly extended distribution of the 658 GHz emission poses a challenge for current maser pumping models.

Richards noted that one surprise from the analysis of these new H_2O maser data is that if it is assumed that dust that forms at 5–10 $R_{\star}$ (as current models predict), this should produce fairly rapid wind acceleration, in contrast to the far more gradual acceleration that is observed. Richards postulated that this implies either that the dust forms more slowly than previously thought, or that it undergoes some kind of annealing or "reorganization" within the wind. She reported seeing a similar trend in other stars as well. A. Zijlstra suggested an alternative possibility, namely that asphericity, together with velocity variations related to the time-variable mass loss, may imprint similar signatures on the outflow.

On a related point, Zijlstra questioned the strength of current evidence for dust-driven winds in RSGs. K. Gayley pointed out that confoundingly, temperatures are only cool enough for dust to form at relatively large radii in RSGs, seemingly too far out to drive the wind. He suggested that perhaps molecular opacity from molecular layer or "MOLsphere" (Tsuji 2000, 2001) could play a role. V. Strelnitski drew attention to previous work by his team that showed this may be plausible for C-rich giants and for some O-rich giants (Shmeld et al. 1992; see also Jorgensen & Johnson 1992; Helling et al. 2000). However, the precise role of molecular opacity remains an open question, and the topic appears to have received relatively little recent attention. Overall there does not appear to be a present consensus on the driving mechanism for RSG winds (see also Section 9).

Other results from the analysis of Richards's team included evidence favoring a time-variable mass-loss rate, and the need for gas clumps $\sim$50 times denser than previously suspected to explain the observed patterns of spatial overlap between various H_2O maser lines. Richards noted that in future 22 GHz H_2O maser observations from e-MERLIN it will be possible to detect the stellar continuum along with the H_2O maser emission and thus astrometrically align the two. Such precise spatial registration between the masers and the star will enable placing even more stringent constraints on pumping and dynamical models (e.g., Gray et al. 2016).

High-resolution studies of the continuum (radio photosphere) have already been performed for another RSG, Betelgeuse (Richards et al. 2013; O'Gorman et al. 2017). The

recent ALMA study of O'Gorman et al. with 14 mas resolution made it possible to discern thermal structure, including a region ~1000 K brighter than the mean disk, indicating localized heating.

13. Studies of Stars at Ultra-high Angular Resolution

13.1. Very Long Baseline Interferometry

A. Mioduszewski (NRAO) reviewed the many aspects of stellar astrophysics that can be advanced by the ultra-high angular resolution measurements achievable with VLBI. A key advantage of this technique comes from the relevant physical scales that can be probed. For example, for a fiducial 5000-mile (8600 km) baseline, the achievable angular resolution at 20 cm and 7 mm is ~5 mas and 0.17 mas, respectively. (Note that 1 mas corresponds to ~1 au at a distance of 1 kpc and to $\sim 10\,R_\odot$ at $d \approx 100$ pc). In addition, astrometric precision of $\lesssim$50 μas in VLBI positional measurements is now routine (e.g., Forbrich et al. 2016a; Ortiz-Léon et al. 2017). On the other hand, a drawback of VLBI is that the brightness temperature sensitivity scales with baseline length $B_{\rm max}$ as: $T_B = 0.32\sigma_N\left(\frac{\rm mJy}{\rm beam}\right)B_{\rm max}({\rm km})^2$, and for present VLBI arrays, the achievable noise level (σ_N) typically limits this technique to sources with $T_B \gg 10^4$ K. Thus VLBI is sensitive only to compact, nonthermal emission (e.g., masers, synchrotron, ECM) or thermal sources seen in absorption against nonthermal backgrounds.

Mioduszewski summarized ongoing work by her team to study the radio emission from the weak-lined T Tauri binary V773 Tau (see also Section 4). They find the radio emission to be extremely variable (by factors of 5 or more), with significant brightening occurring near periastron, providing further evidence that PMS stars that produce nonthermal continuum emission are interacting. Additionally, in her team's Gould's Belt VLBA distance survey of young stars (Ortiz-Léon et al. 2017 and references therein), over 50% of those PMS stars with nonthermal emission are confirmed close binaries, suggesting that close pairings help to create conditions conducive to the production of such radio emission. However, the exact mechanism through which the nonthermal emission is unhanced is unclear.

Position shifts of the two V773 Tau components are seen near periastron, suggesting that when the stars are far apart, their radio centroids correspond to the stars themselves, but when they are close together, the emission arises from a region in between. Recent follow-up observations with the High Sensitivity Array by Mioduszewski and her group show evidence for a bright connecting feature between the stars after they begin brightening near periastron. The changes are very rapid, consistent with a possible magnetic reconnection-type event.

Mioduszewski concluded her talk with a look forward to the future of VLBI. In the near term, the VLBA is returning to the NRAO's portfolio, and options are being explored to increase VLBA bandwidths to 2 GHz, improving sensitivity by a factor of three. Discussions are also underway to include in plans for the ngVLA an upgrade of existing VLBA sites with ngVLA technology, along with the possible introduction of additional intermediate baselines to bridge ngVLA and (current) VLBA baselines (Murphy et al. 2018; Reid et al. 2018). Such a plan could result in more than a factor of 100 improvement in sensitivity over the current VLBA and improve sensitivities to the point that brightness temperatures of $T_B \sim 1000$ K (i.e., thermal sources) would be within reach. This would provide resolution of $<0.3\,R_\odot$ at 50 GHz, making it possible to image the disks of the 100 closest stars. Elsewhere, cm-wave VLBI stations are being deployed in Africa to form part of an African VLBI network (e.g., Copley et al. 2016) that is expected to play a crucial role in enabling VLBI with the SKA.

13.2. New Image Reconstruction Methods

K. Akiyama (MIT Haystack Observatory) showcased a powerful new image reconstruction technique for radio interferometry applications known as "sparse modeling" (Honma et al. 2014). This technique has been shown to achieve image resolution up to ~0.3× the nominal diffraction limit, but with substantially better fidelity than traditional CLEAN deconvolution. While recent sparse modeling developments and applications have focused primarily on the needs of mm VLBI experiments (Akiyama et al. 2017a, 2017b), Akiyama showed that sparse modeling has a variety of other potential applications where maximum angular resolution and high image fidelity are important, including the imaging of circumstellar disks and stellar surfaces. As one illustration, he presented a sparse model reconstruction of the radio photosphere of the AGB star Mira based on ALMA data from Matthews et al. (2015; see also Matthews et al. 2018; Section 11.1). The resulting image reveals low-contrast surface features that cannot be discerned directly from images made using CLEAN deconvolution.

14. Evolution Beyond the AGB

In his review talk, A. Zijlstra issued a reminder that we still lack a robust formalism for describing how low-to-intermediate mass stars evolve from the AGB to the post-AGB and PN stages. Still unsolved questions include how the shell of the star gets ejected, what are the maximum mass-loss rates achieved during this process, and what are the timescales for the various processes involved. Underscoring this latter question, Zijlstra pointed to the recent models of Miller Bertolami (2016) whose refined evolutionary timescales differ by a factor of three or more compared with most earlier models.

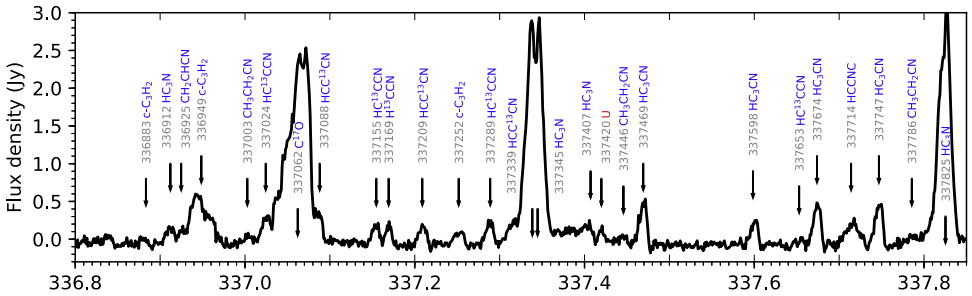

Figure 6. Sample portion of the SMA spectrum of the pre-PN CRL 618 obtained by Patel et al. (2018 and in preparation). The frequency axis is in GHz. Lines labeled with a "U" are unidentified.
(A color version of this figure is available in the online journal.)

14.1. The Post-AGB and Pre-PN Stages

Because stars transitioning from the post-AGB into PNe evolve considerably over timescales of only a few thousand years, observable variations in the radio emission linked with source evolution are expected. This has been observed in the case of the very young PN NGC 7027 by Zijlstra et al. (2008), who were able to use multi-frequency radio observations, coupled with model fits, to derive an extremely precise mass estimate for the central star. On the other hand, Zijlstra cited other cases where the observed radio variability in similar objects is not straightforward to interpret. For example, Cerrigone et al. (2017) identified a few sources evolving toward PNe that showed either increases or decreases in the radio flux over the course of ∼10–20 years, but it is unclear if these mirror the ionization changes expected from source evolution or simply variability of the central star. For the pre-PN CRL 618 (see also below), Sánchez-Contreras et al. (2017) recently found evidence that the long-term variability may be periodic.

Another important effect that occurs during the AGB → PN transition is that ionizing photons from the central star begin to alter the chemistry of the circumstellar material. Shocks linked with the bipolar outflows that may appear during this time can also impact the chemistry. N. Patel (CfA) described his team's recent program to study the astrochemistry of objects spanning the transition from the post-AGB to PNe in order to better characterize these changes and test theoretical predictions (e.g., Bachiller et al. 1997). Their work takes advantage of the new wide bandwidth SWARM correlator on the SMA (Primiani et al. 2016), which provides up to 32 GHz instantaneous bandwidth with 140 kHz spectral resolution.

As Patel explained, surveying these wide bandwidths is crucial, as many molecules (e.g., H_2CO, CH_3CN) emit lines spread out over a wide swath of frequency. In cases where the lines are optically thin, obtaining simultaneous measurements of multiple lines enables construction of population diagrams (e.g., Lee et al. 2013), which in turn yield measurements of both the excitation temperature and column density. As Patel showed, this method is also useful to confirm line identifications and identify lines that may be blended (a significant problem at submm wavelengths).

As an example of his group's recent work, Patel presented spectra of CRL 618 obtained with the SMA from 282–359 GHz (Patel et al. 2018; Figure 6). This source has outflows spanning tens of arcseconds, but Patel's team focused on the inner few arcseconds, where they were able to detect a total of 1075 lines, 373 of which are presently unidentified. The detections included a number of H RRLs that were spatially unresolved by the 0.″5 beam. With the exception of SiO(8-7), no Si-bearing molecules were detected. In comparison, Patel noted that only 440 lines were detected toward the highly evolved C-rich AGB star IRC +10216 over a similar frequency range (Patel et al. 2011). However, while the number of lines detected toward CRL 618 is larger, the number of distinct molecules is far smaller than in IRC+10216. Indeed, the majority of the CRL 618 lines arise from just two molecules, HC_3N and c-C_3H_2. Patel also reported that line survey data have been obtained for NGC 7027 over a ∼60 GHz band, but in this case, only 26 lines were detected.

Patel's group is currently working with laboratory spectroscopists to reconcile many of the unidentified lines toward their target sources. Preparations are also underway to perform a wide bandwidth survey the young PN CRL 2688 with the SMA in 2018. Patel noted that future work at lower (cm-wave) frequencies, which are sensitive toward larger molecules and longer carbon chains, would be an important complement to his team's SMA studies of young and pre-PNe.

14.2. Planetary Nebulae (PNe)

At cm wavelengths, typical flux densities for Galactic PNe range from ∼1–1000 mJy, and over the last few decades there have been many radio surveys of these objects (e.g., Zijlstra et al. 1989; Chhetri et al. 2013). A recent survey of the Large Magellanic Cloud has also led to the first radio detections of PNe outside the Milky way (31 in total; Leverenz et al. 2017). A key advantage of radio wavelength studies of

PNe is the ability to overcome the the obscuring effects of dust. However, as Zijlstra reminded us, a number of puzzles persist concerning the radio properties of these object.

14.2.1. The Origin of the Shapes of PNe

As summarized by Zijlstra, it has become clear that much of the complex structure observed in PNe must originate from the effects of binary companions. Wide binaries can produce modest levels of gravitational focusing, leading to elliptically shaped nebulae; closer companions can produce more active shaping and lead to the formation of disks and jets; and finally, a very close-in companion (as occurs in ∼5% of cases) can lead to common envelope ejection—the least understood of the binary scenarios. Zijlstra noted that presumed "single-star" PNe (that are roughly spherical) do exist, but they are rare, comprising ∼20%–30% of PNe. These are typically more difficult to find, as they are on average fainter owing to the absence of binary-induced density enhancements in their ejecta, but Zijlstra predicted that more will be found in deeper surveys.

14.2.2. Synchrotron Emission from PNe

As both radio emission and Hβ emission arise from free–free processes, the ratio of these two tracers should provide a straightforward measure of the extinction. Nonetheless, there remains a persistent disagreement in the extinction so inferred as compared with estimates from the ratio of Hα/Hβ: the radio fluxes are consistently too low. For years this was attributed to the adoption of a standard Galactic ratio of total-to-selective extinction ($R_V = 3.1$) toward the Bulge, which may not be valid (Ruffle et al. 2004). However, this has been disputed by Pottasch & Bernard-Salas (2013), who instead argue that the 6 cm radio fluxes are discrepant by up to a factor of two because of missing optically thick emission (e.g., from clumpy material). This remains an ongoing controversy.

Another open question is whether or not PNe emit synchrotron radiation as a result of shocks induced by the hot wind of the central star—an idea first suggested by Dgani & Soker (1998). Zijlstra noted that to date, no such emission has ever been detected from within a PN, although the expected signal (∼1 mJy for a source at 1 kpc and $\nu = 1$ GHz) would be difficult to discern when superposed on the much brighter free–free emission. Bains et al. (2009) detected variable nonthermal emission from 3 out of 28 post-AGB stars surveyed, hinting that such emission may only occur before the nebula is ionized (see also Pérez-Sánchez et al. 2013, 2017). Yet another related object is V1018 Sco, which appears to be an OH/IR star with associated synchrotron emission and PN emission (Cohen et al. 2006) and Zijlstra urged further studies of this enigmatic object. He also noted that future surveys capable of measuring flux variability at the μJy level could in turn allow measurements of the expansion of many PNe, as well as the derivation of their central star masses, providing a key missing ingredient in models of AGB evolution.

14.2.3. Enigmatic X-ray Point Sources

One more outstanding puzzle concerns the X-ray point sources seen in approximately half of the PNe that are detected in X-rays. Of these, ∼15% show hard X-rays. Zijlstra and his collaborators find that at least some of these cases may be attributed to an (old) main-sequence companion that has been rejuvenated by the AGB wind (Montez et al. 2015). However, efforts to detect the predicted weak radio emission from these sources (expected to be $\sim 1\,\mu$Jy) have been unsuccessful, mostly likely due to sensitivity limitations. So far there are no obvious trends seen in the ages or nebular morphologies of the PNe containing the hard X-ray sources.

14.2.4. Radio Recombination Lines (RRLs) in PNe

Zijlstra noted that RRLs in PNe are relatively little observed because they tend to be weak and relatively broad (∼15 km s^{-1} thermal motions), making it difficult to use these lines for dynamical measurements. Nonetheless, he emphasized that they are excellent tracers of obscured regions. He also noted that there are a few cases known where masing is seen near the H30 lines, which appear to be linked with rotating disks (Sánchez-Contreras et al. 2017; Aleman et al. 2018). Angular momentum arguments then dictate that a binary companion must be present. Zijlstra predicted that studies of RRLs in PNe will be facilitated by the increased collecting area of future telescopes such as the SKA.

14.2.5. Molecules in PNe

Zijlstra pointed out that most molecules are typically found only in young PNe, although CO tends to be found in PNe over a wide range of ages. This includes cases where it is seen in an outer shell (e.g., NGC 7027) or in cometary globules which can shield it (e.g., the Helix). ALMA has recently enabled the mapping of CO in PNe in unprecedented detail, leading to a number of surprises. In the young PN M2-9, Castro-Carrizo et al. (2017) recently identified two CO rings separated by a gap, most likely as a result of mass-loss events separated by ∼500 yr. The cause of these discrete events is not entirely clear, although a binary companion has been implicated. In the case of the Boomerang nebula (which is so cold that it has been observed in absorption against the cosmic background radiation) CO is seen to trace both polar lobes and an expanding torus (Sahai et al. 2017). This may be the result of a common envelope system, although Zijlstra questioned whether such systems can drive jets, as observed in this source. Finally, in the PN NGC 6302, Santander-García et al. (2017) were able to uncover a second inner ring, inclined to a previously discovered expanding molecular torus. The former appears to

have an age (∼2000 yr) similar to ionized lobes that are also seen. This again suggests a double ejection event took place.

14.2.6. $^3He^+$

$^3He^+$ is a product of the *p-p* cycle within low-mass stars, and is only dispersed when these stars reach the end of their lives, making it the last addition to the baryonic universe. But how much $^3He^+$ solar-mass stars contribute depends very sensitively on stellar interior processes during the red giant branch and AGB phases (e.g., how much mixing occurs and how much $^3He^+$ gets destroyed inside the star).

$^3He^+$ can be studied through a rather weak spin-flip transition at 8.6 GHz, and so far it has been detected in three PNe (Balser et al. 1997, 2006; Guzman-Ramirez et al. 2016). All show a double-peaked line profile, in contrast to the centrally peaked RRLs seen in these same objects. The abundances are also higher than expected, and the $^3He^+$ line appears significantly brighter than predicted. This can be accounted for neither by cosmological models nor stellar nucleosynthesis. A possible explanation recently proposed by Zijlstra and his collaborators is that the $^3He^+$ line is masing, possibly as a result of pumping by $^4He^{++}$ recombination (Guzman-Ramirez et al. 2016). If true, this will make results derived from the $^3He^+$ line much more difficult to interpret.

15. White Dwarf Binaries

15.1. Cataclysmic Variables (CVs)

Cataclysmic variables (CVs) are binary systems containing a white dwarf accreting mass from a low-mass, main-sequence companion of M or K spectral type. CVs are further divided into magnetic ($B \gtrsim 10^6$ G) and non-magnetic systems ($B \lesssim 10^6$ G) based on the field strength of the white dwarf. A review talk by D. Coppejans (Northwestern University) described how the increased sensitivity of modern radio interferometers has enabled a steady stream of discoveries related to CVs within the past few years.

Coppejans noted that as of the 1980s, only 4% of non-magnetic CVs (three systems in total) had been detected in the radio. This led to the surprising inference that CVs do not launch jets (Soker & Lasota 2004), which would make them a rarity among accreting sources. However, this problem was revisited by Körding et al. (2008), who looked at the dwarf nova SS Cyg during its (optical) outburst phase and discovered radio emission attributed to synchrotron radiation from a transient jet. In a more recent study by Mooley et al. (2017) with the Arcminute Microkelvin Imager Large Array, data obtained over the course of one week not only confirmed this behavior, but showed the spectral index of SS Cyg changing from positive to negative as the jet evolves, plus the first ever detection of a luminous flare near the end of the outburst.

Following the most recent VLA upgrade, Coppejans led a campaign to re-observe four nova-like CVs that were previously undetected in the radio. Three of the four were detected at 6 GHz during multiple epochs (Coppejans et al. 2015). Their emission was found to be variable and circularly polarized, indicating that it could not be purely thermal in nature. For one target, TT Ari, the radiation was nearly 100% circularly polarized, implying a coherent emission component that is suspected of being ECM. Coppejans noted that the emission from this source is reminiscent of magnetic CVs (cf. Barrett et al. 2017). However, the interpretation is not straightforward, since the secondary in this system is an M3.5 dwarf, which may be prone to flaring. TT Ari's radio luminosity is nearly two orders of magnitude brighter than typical flares for field dwarfs, but the secondary is tidally locked into an orbit with a period of 3.5 hours, implying a rotation velocity of ∼160 km s^{-1}—considerably faster than field stars—which may lead to stronger flares. R. Osten also pointed out that in contrast to X-ray emission, there is no saturation level for the radio luminosity of flares, and at least one flare of comparable luminosity to the TT Ari flares ($\sim 10^{16}$ erg s^{-1} Hz^{-1}) has already been detected from a field M dwarf in a wide binary (Osten et al. 2016).

Another recent study led by Coppejans aimed to examine the behavior of radio emission from CVs during optical outbursts. Such comparisons are challenging, since these events occur unpredictably, and the radio emission is expected to peak within 24 hours of the outburst. To circumvent this, her team monitored a sample of CVs to identify outbursts and enable rapid triggering of radio wavelength follow-up with the VLA. In total, they obtained follow-up observations of five outbursting CVs at 8–12 GHz. All were detected with specific radio luminosities in the range $L_{10\mathrm{GHz}} \sim 10^{14} - 10^{16}$ erg s^{-1} Hz^{-1} and were found to exhibit variable radio emission on timescales ranging from 200 s to several days (Coppejans et al. 2016; Figure 7). No correlation was found between the radio luminosity and any other properties of the CVs, but Coppejans emphasized that this should be further explored with higher cadence radio monitoring (sampling times of order hours, not days) since the objects are so highly variable.

Until recently, another unsolved question has been whether the observed radio emission from CVs is dependent on their accretion state. Coppejans reported that based on some recent analysis by her team, the answer is "yes", as none of the CVs they have observed with the VLA have been detected during quiescence. This seems to support a jet model for the emission, but Coppejans cautioned that additional observations are needed to establish the actual fraction of CV outbursts that are radio-loud.

Another result highlighted by Coppejans was the recent discovery of the first "white dwarf pulsar", AR Sco (Marsh et al. 2016; Buckley et al. 2017). Marsh et al. monitored this binary over a wide range of wavelengths, including optical, IR,

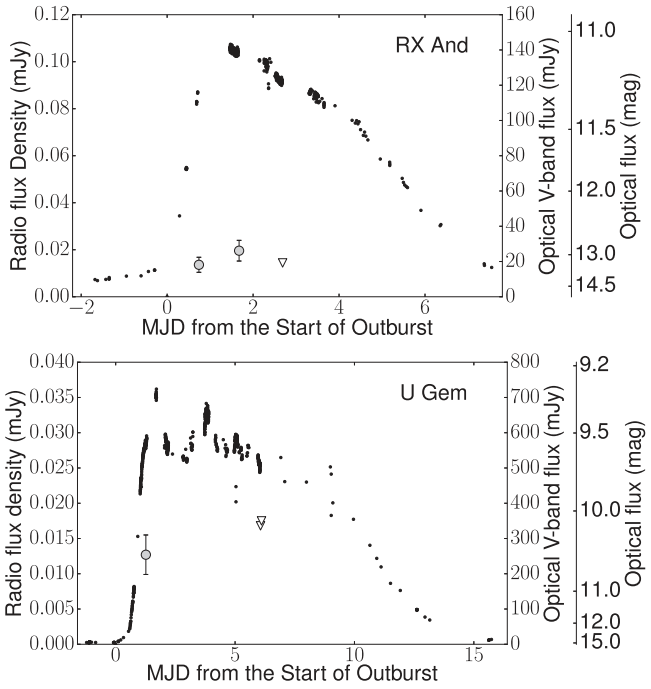

Figure 7. Radio and optical light curves during the outbursts of two dwarf nova-type CVs. The 10 GHz radio data obtained with the VLA are shown as grey symbols (triangles for upper limits). *V*-band optical data are shown as black dots. The *x*-axis indicates elapsed time in modified Julian date. Adapted from Figure 1 of Coppejans et al. (2016) with permission of Oxford University Press.

and 9.0 GHz radio continuum with the ATCA, leading to the discovery of pulsed emission with a period of 1.97 min in all wavelength bands. The broadband radio emission is thought to be synchrotron radiation produced by the interaction of the spinning white dwarf with the coronal loops of the M dwarf companion. Although AR Sco is presently a unique system, Coppejans suggested it may represent a common evolutionary phase for CVs and may ultimately evolve into a magnetic CV.

Future radio studies of CVs are expected to be enabled by ThunderKAT (Fender et al. 2017), a transient survey slated to be carried out commensally on the MeerKAT array (Jonas 2009). In addition, Coppejans is part of a team with 250 dedicated hours for CV work on MeerKAT. She noted that a 1 m optical telescope (MeerLICHT) will be slaved to MeerKAT to provide simultaneous, multi-band optical observations of every field studied. Coppejans urged consideration of a similar facility in plans for the ngVLA.

15.2. Classical Novae

Classical novae are accreting binary systems (either CVs (see Section 15.1) or symbiotic systems) that exhibit thermonuclear runaway on the surface of a white dwarf, leading to a non-recurring ejection of large amounts of material. Approximately 35 classical novae occur each year in the Galaxy, out of which typically ∼8 are observed. M. Rupen (National Research Council, Canada) summarized the rapid growth in discoveries related to these objects thanks to recent radio observations.

The long-prevailing paradigm for understanding the evolution of classic novae is one where the ejecta are analogous to an H II region (powered by the hot white dwarf), and where the ejected material undergoes a homologous ("Hubble flow") expansion. In this model, the radio emission is thermal bremsstrahlung, and the radio light curve is characterized by an optically thick rise with time t ($t^2 \propto \nu^2$) and an optically thin decay ($t^{-3} \propto \nu^{-0.1}$). On the basis of this predicted behavior, it is possible to directly estimate the mass of the ejecta, although historically such masses have been systematically larger than theoretically predicted. Clumping in the ejecta has been invoked to reconcile this discrepancy (e.g., Wendeln et al. 2017), but clumping models are poorly constrained.

While the aforementioned paradigm has been relatively successful, Rupen noted that cracks have begun to appear, thanks in large part to the results of recent radio studies. He presented emerging evidence in favor of a revised picture where shocks play a dominant role and where at least two distinct outflows occur from a single source.

A significant problem for the "H II region" model of classical novae is that free–free emission alone cannot fully account for recent radio measurements. In a study of the 2015 nova V1535 Sco by Rupen's team (Linford et al. 2017), the optical data appear to adhere to the classic model, while the radio data show a wide range of complex behaviors. Radio light curves measured at various frequencies show significant fluctuations rather than smooth evolution, with the behavior differing between the frequency bands. Rupen suggested that this may be a consequence of shocks between material from different ejection phases. The radio SEDs also vary from day to day, and on several days exhibit slopes that can only be explained by synchrotron radiation ($\alpha = -0.36$ to -0.88). Furthermore, imaging of the source reveals $T_B > 6 \times 10^5$ K. To account for such high temperatures from thermal emission alone would require far more emitting material than is inferred from concurrent X-ray measurements. Another source studied by Rupen's team, V1723 Aql, showed an unexpectedly rapid turn-on in the radio, an anomalous spectral index ($\alpha \propto \nu^{1.3}$), a double-peaked radio light curve, and $T_B > 10^6$ K (Weston et al. 2016b). A double-peaked radio light curve was also seen in V1324 Sco (Finzell et al. 2018).

Rupen reported that there are now at least 9 classical novae known to emit γ-rays, and these statistics are consistent with all novae being γ-ray emitters. While an association between synchrotron emission (shocks) and the emission of γ-rays seems likely, an outstanding puzzle is why some sources such as V1324 Sco show γ-rays but no X-rays, while others (e.g., V5589 Sgr) show hard X-rays (another shock tracer) but are undetected in γ-rays (Weston et al. 2016a). It is presently

unknown if these differences can be explained by variations in geometry/viewing angle.

A first major clue came from the study of V959 Mon, a nova that was detected in γ-rays and for which follow-up radio light curves and VLBI imaging at multiple epochs were obtained (Chomiuk et al. 2014). The model that emerged is one where there is a slow shell ejection early on. Interaction with the companion then leads to enhanced mass loss perpendicular to the orbital plane. Later, fast ejection occurs in an orthogonal direction, shaped by the initial torus, and shocks occur between the early and late winds. Subsequently, the fast ejecta fade away, leaving behind the more slowly moving material. However, Rupen stressed that there is still considerable work to be done to gain a more comprehensive understanding of classical novae. He noted that to confirm or refute the new emerging paradigm for understanding these objects, it will be crucial to study additional novae with the type of high-quality detailed data that were obtained from V959 Mon. The processes that might lead to a two-phase ejection are still unclear, as is the reason for deviations from the expected rate of rise of the radio light curves. Rupen concluded by pointing out that the combined sensitivity and angular resolution of the ngVLA would make it an ideal instrument for pursuing this topic.

15.3. "Red" Novae

T. Kamiński (CfA) presenting recent findings concerning the enigmatic nova-like object CK Vul (Nova 1670) based on mm and submm observations (Kamiński et al. 2018). The appearance of this source was first recorded in 1670, and in the two years following, it underwent three distinct episodes of brightening after which it appeared extremely red to the naked eye. CK Vul's inner nebular remnant was first detected in the 1980s (Shara et al. 1985), and a more extended "hourglass" nebula was later uncovered by Hajduk et al. (2007). No stellar remnant has so far been identified, although there is a weak radio source at the center of the bipolar nebula.

Recently, Kamiński and his collaborators obtained spectroscopic observations of CK Vul using the Atacama Pathfinder EXperiment (APEX) and IRAM 30 m telescopes, as well as interferometric imaging using the NOrthern Extended Millimeter Array (NOEMA), the SMA, and ALMA. These observations revealed a multitude of emission lines, leading to the identification of over 320 unique spectral features (Kamiński et al. 2017). The observed linewidths are typically $\sim$300 km s^{-1}—far smaller than in classic novae—and the interferometric images show considerable kinematic complexity, including jets, rings, and wide-angle outflows. Large quantities of dust are also present, with temperatures of a few tens of K. By analyzing the full SED, it was possible to derive a luminosity of the central source ($\sim$0.9 $L_{\odot}$) and a total mass for the remnant (gas+dust) of $\sim$0.1 $M_{\odot}$ (Kamiński et al. 2015).

The collection of molecules detected in CK Vul is highly unusual; N and F appear overabundant, and the species include some typically seen only in either C-rich or O-rich environments. Perhaps most surprising is that for nearly all of the molecules detected, rare isotopologues are also seen, and all of the CNO isotopes are significantly enhanced relative to solar composition.

Having such rich information about the isotopologue ratios in CK Vul enables placing new constraints on its progenitor. Kamiński's team finds that the abundances can be explained neither as the products of nucleosynthesis nor a classical nova event. Instead, the object's origin is suspected of being a stellar merger (Tylenda et al. 2013; Kamiński et al. 2015), and based on recent findings, CK Vul is now believed to be being one of a small but growing group of objects dubbed "red novae."

Another noteworthy feature of CK Vul is its anomalously high abundance of the radioactive nucleotide ^{26}Al, which is observed as part of the isotopologue ^{26}AlF. Kamiński emphasized that this is also important in a broader astrophysical context, since the decay of ^{26}Al into Mg produces a γ-ray line at 1.8 MeV. This line has long been observed by γ-ray telescopes, pointing to an as-yet unidentified source of ^{26}Al in the Galaxy. CK Vul represents the first astronomical object in which ^{26}Al has been directly identified. While CK Vul-like objects alone are too rare to account for all of the ^{26}Al seen by γ-ray telescopes, Kamiński predicted that radio telescopes may soon uncover additional sources of this isotope.

16. Radio Stars as Denizens of the Galaxy

16.1. Stellar Populations in the Galactic Center

There has been longstanding interest in the stellar populations in the neighborhood of Sgr A*, the black hole at the Galactic Center (GC). Material shed by the winds of mass-losing, massive OB stars near the GC are expected eventually feed onto Sgr A*. There has also been speculation as to whether star formation can proceed in situ within the extreme environment close to the black hole. As noted by M. Rupen, understanding the initial mass function in this region is also relevant to understanding star formation in the extreme environments present in submillimeter galaxies (e.g., Safarzadeh et al. 2017). However, as described by F. Yusef-Zadeh (Northwestern University), only recently has radio emission been detected and resolved from individual stars within the GC region (e.g., Yusef-Zadeh et al. 2015a). He summarized results from several such studies.

Taking advantage of the wide (8 GHz) continuum bandwidths now available with the VLA at 34 and 44 GHz, Yusef-Zadeh's group has now detected over 300 compact radio sources within 30″ of Sgr A*, including 30 of the 90 massive stars with previously known IR counterparts (Yusef-Zadeh et al. 2015a). For those stars, mass-loss rates derived from radio and IR were compared. After accounting for wind clumping,

the radio measurements are systematically an order of magnitude lower ($\dot{M} \sim 10^{-7}\,M_{\odot}\,\mathrm{yr}^{-1}$), implying a lower accretion rate onto Sgr A* compared with previous estimates. Yusef-Zadeh argued that the radio estimates of $\dot{M}$ are likely to be the most reliable because of the need for fewer assumptions (see also Section 10.1).

The same VLA survey also uncovered ∼50 compact, partially resolved radio sources with associated bow shocks, and some cases, cometary-like tails that align toward the massive stars in the region. These partially resolved sources do not have IR counterparts, and Yusef-Zadeh et al. (2015b) have identified them as probable proplyds. The corresponding size scales (∼500 au) are consistent with this interpretation. Furthermore, arguments concerning both the evaporation timescales and the stability against tidal disruption imply that these objects must be self-gravitating and cannot be merely clumps of ionized gas. A surprising implication is that low-mass star formation is ongoing in the neighborhood of Sgr A*. Follow-up ALMA observations also uncovered dust from these objects (Yusef-Zadeh et al. 2017a) and enabled mass determinations of the disk components (0.03–0.06 $M_{\odot}$). The estimated ages are $\sim 10^5$–10^6 yr—far younger than the neighboring massive star cluster, whose age is a few million years.

Another population of sources uncovered by Yusef-Zadeh's group within a pc of Sgr A* comprises 11 objects exhibiting signatures of bipolar outflows (Yusef-Zadeh et al. 2017c). ALMA observations in spectral lines including ^{13}CO(2-1) show unambiguous signatures of red- and blue-shifted gas lobes centered on a compact central source (Figure 8). Inferred dynamical ages of ∼6500 yr again point to the ongoing formation of low-mass stars in this extreme environment. Yusef-Zadeh stressed that the bipolar sources and proplyds found near the GC mark the first time that individual low-mass YSOs have been directly detected at such large distances (>8 kpc) and that this only possible at radio wavelengths.

Finally, Yusef-Zadeh described an enigmatic source in the GC known as IRS 3 (Yusef-Zadeh et al. 2017b). Whether this is dusty YSO or an AGB star is currently unclear, although the latter classification is presently favored based in part by detection of a shell-like structure of ^{13}CO emission surrounding the star. Numerical simulations show that the non-spherical shape and extended size of the object (∼8000 au) can be explained by tidal distortion of an extended radio photosphere.

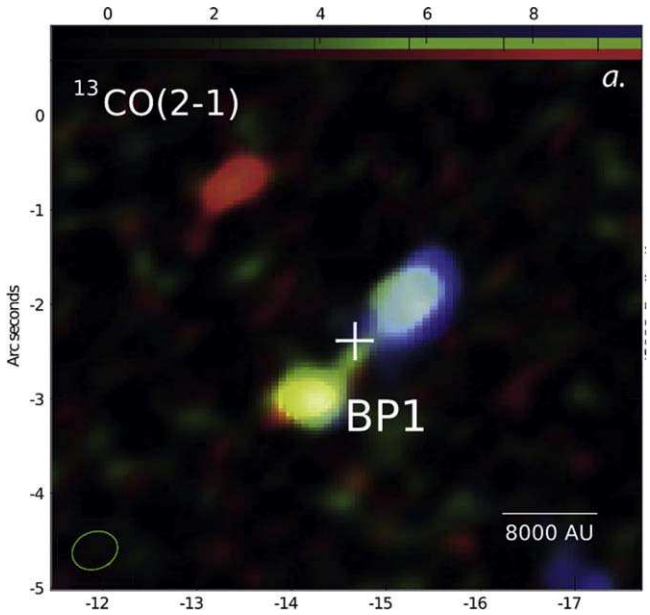

Figure 8. Example of a YSO detected at a projected distance of ∼0.6 pc from Sgr A* in deep ALMA observations. The two lobes of ^{13}CO(2-1) emission are red- and blueshifted by ∼2 km s^{-1} and are connected by intermediate velocity gas. The intensity range is between −1 and 10 mJy beam^{-1}. The cross marks the position of a compact 226 GHz continuum source. Reproduced from Yusef-Zadeh et al. (2017c). © AAS.
(A color version of this figure is available in the online journal.)

16.2. Mapping the 3D Structure of the Galaxy

Y. Pihlström (University of New Mexico) reviewed recent efforts to use molecular maser emission from large samples of evolved stars to provide new information on the structure and dynamics of the Milky Way. She is a key team member of the BaADE project (Trapp et al. 2018; see also Section 12.3), which is aimed at making significant leaps in our understanding of the bulge and bar regions of the Galaxy, including the question of whether the Milky Way's bulge was formed early in its history, or later by buckling of the disk.

As discussed by Pihlström, far-IR colors based on measurements from the *Infrared Astronomical Satellite* (*IRAS*) provided the first efficient means of identifying large samples of low-mass, evolved stars within the Galaxy, and follow-up observations of many of these stars in maser lines (including OH and SiO) subsequently provided crucial line-of-sight velocity information for mapping Galactic structure (te Lintel Hekkert et al. 1991; Deguchi et al. 2014a, 2014b). However, previous sample selection toward the bulge and plane was severely restricted by confusion and high extinction, leaving too few stars to derive detailed structural and dynamical information.

A major advantage for BaADE is an improved method to identify larger numbers of SiO maser stars. Using mid-IR color data from the *Midcourse Space eXperiment* (*MSX*), which had a beam of ∼2″ and which focused on the Galactic Plane, Sjouwerman et al. (2009) found a high success rate in detection of SiO masers (∼50%–90%). In total, 28,000 candidate evolved stars were identified as targets for follow-up SiO observations; ∼19,000 have now been observed at 43 GHz with the VLA (totaling over 400 hours), and ∼9000 stars (those too far south for the VLA) are currently being targeted at

86 GHz with ALMA. Multiple SiO transitions/isotopologues are covered in the observing bands, along with a few lines from C-bearing molecules that can be used to obtain velocities for C-rich AGB stars lacking SiO lines.

Observations remain ongoing, but the new data have already dramatically increased the sampling of the Galactic potential compared with past surveys. Measured dispersions allow separating the sample stars into disk and bulge populations. Evidence for cylindrical rotation is clearly seen. Future work will include follow-up VLBI astrometry for select stars to obtain parallaxes and proper motions. The current database of over 20,000 SiO maser sources will also enable statistical studies of maser pumping (through comparison of different lines) and of the correlations between the maser properties and other properties of the stars themselves (see also Section 11.2). Follow-up IR spectroscopy is planned to obtain metallicity information for the sample.

Pihlström noted that BaADE complements the BeSSel Survey of Reid et al. (2014), which used H_2O and CH_3OH maser measurements of high-mass star-forming regions to determine the positions of spiral arms within the Galaxy (see also Sanna et al. 2017) and to measure parameters such as the Galactic rotation speed and distance to the GC. Radio measurements like these also provide an important complement to optical astrometry for understanding stellar populations, Galactic structure, and the dynamical evolution of the inner Galaxy. L. H. Quiroga-Nuñez (Joint Institute for VLBI European Research Infrastructure Consortium/University of Leiden) described one such project, aimed at studying the population of SiO maser-emitting bulge stars from BaADE for which complementary measurements exist from *Gaia* and other optical/IR surveys. Quiroga-Nuñez's team plans to select a subset of these stars for astrometric VLBI follow-up to enable direct comparisons between astrometry obtained using radio and optical methods (Quiroga-Nũnez et al. 2018). The VLBI measurements are expected to achieve 3D orbits and parallaxes with 50 μs accuracy, comparable to *Gaia*. In addition, his team plans to obtain VLBI astrometry for stars that are too optically bright ($g < 9$) to permit *Gaia* astrometry.

17. Radio Star Surveys—Current and Future

G. Umana (Istituto Nazionale de Astrofisica/Observatatorio Astrofisico di Catania) noted that we presently do not have a satisfactory answer to a question frequently posed extragalactic astronomers, namely "How many sub-mJy stellar sources are expected (above a certain detection threshold) within one square degree of sky?" She pointed out that there are presently no good statistics on the detectability of radio emission from various classes of stars, since existing survey data provide few useful constraints; they are typically too shallow to detect stellar sources, have poor angular resolution, and/or concentrate only on high Galactic latitudes. Furthermore, to date, very few stars with luminosities comparable to the Sun have been detected at cm wavelengths, and those that have have required many hours of integration (e.g., α Cen A and B; Trigilio et al. 2018; τ Cet, η Cas A, 40 Eri A; Villadsen et al. 2014; Section 5). This means that our current information comes primarily from targeted observations.

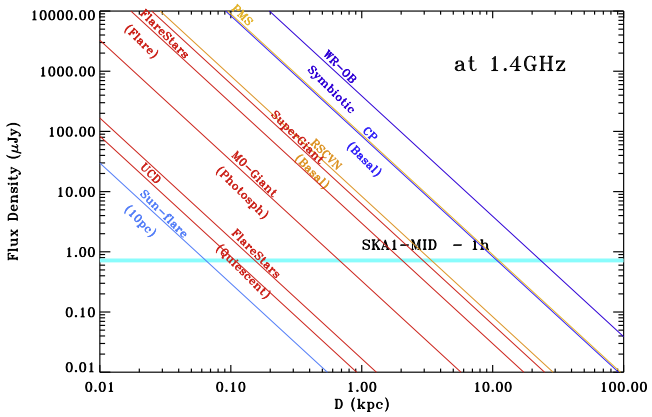

Figure 9. Predicted 1.4 GHz flux densities (in μJy) as a function of distance (in kpc) for various classes of stars. The horizontal line indicates the expected detection threshold for phase 1 of the SKA. Adapted by G. Umana from Umana et al. (2015b).
(A color version of this figure is available in the online journal.)

Umana predicted that the aforementioned limitations will finally be overcome with the next generation of sensitive all-sky radio surveys currently being planned. This will include the Evolutionary Map of the Universe (EMU) survey to be conducted with the Australian Square Kilometre Array Pathfinder (ASKAP; Norris et al. 2011), slated to map 75% of the sky, including the Galactic Plane, at 1400–1800 MHz to a depth of 10 μJy beam^{-1} at 10″ resolution. EMU is expected to detect UCDs to 20–30 pc, RS CnV binaries to 500 pc, and winds from W-R and OB stars to the GC. Eventually, SKA-MID will be able to detect most classes of stars throughout the Galaxy (Figure 9), while SKA-2 would begin to detect many of these classes in nearby galaxies (Umana et al. 2015a).

In the framework of EMU, Umana's team has recently begun a deep radio survey of a 2° × 2° region of the Galactic plane with ∼10″ resolution using the ATCA at 1.1–3.1 GHz. The targeted flux limit is 40 μJy. This project, known as Stellar Continuum Originating from Radio Physics in Our Galaxy (SCORPIO; Umana et al. 2015b, has two main goals: (1) to gauge the scientific potential of deep radio surveys for stellar and Galactic astronomy and (2) to serve as a technical pathfinder for EMU and future SKA surveys (including how to address issues such as source identification, complexity, variability, and separation from diffuse background emission). Data from a SCORPIO pilot experiment have already been published (Umana et al. 2015b), and among the 614 sources detected, 10 were classified as stars and many remain

unidentified. To improve source classification, Cavallaro et al. (2018) have developed automated pipelines to exploit spectral indices, while Riggi et al. (2016) have developed algorithms to improve automated detection of extended sources. Another ongoing effort seeks to use a combination of radio and IR properties to improve automated classification (A. Ingallinera et al. 2018, in preparation).

I. Stevens also stressed the importance of contemporaneous, multifrequency observations for understanding stars and urged the community to think more about how to carry these out. He drew attention to the opportunity presented by the many current and future radio transient surveys and advocated for piggy-backing to search for bursts of emission for various classes of stars, including OB stars. Stevens further emphasized the need for wide-frequency observations to identify spectral turnovers, coupled with sensitive time-domain studies capable of probing changes on timescales of relevance to studying winds and other stellar processes (∼1 hour or less). Unfortunately, computational limitations presently preclude these kinds of commensal studies with many current interferometers.

While upcoming radio surveys hold exciting promise for stellar astrophysics, S. White sounded a caution that while future survey instruments will be valuable for finding stars, it will be crucial to retain instruments like the VLA and ALMA to enable detailed follow-up studies and to obtain the kinds of time and multi-frequency coverage that are not possible with survey instruments. The meeting concluded with a call to action to insure that this needs gets emphasized among the wider community.

The author gratefully acknowledges the efforts of the RS-2 Local Organizing Committee (H. Johnson, N. W. Kotary, M. Reynolds, and J. SooHoo) and Scientific Organizing Committee (G. Hallinan, R. Ignace, K. Menten, M. Rupen, L. Sjouwerman, and S. White). The author also thanks the anonymous referee for useful comments on this manuscript. Financial support for the RS-2 workshop was provided by a grant from the National Science Foundation (AST-1743708).

References

Ainsworth, R. E., Scaife, A. M. M., Green, D. A., Coughlan, C. P., & Ray, T. P. 2016, MNRAS, 459, 1248
Ainsworth, R. E., Scaife, A. M. M., Ray, T. P., et al. 2014, ApJL, 792, L18
Airapetian, V. S., Adibekyan, V., Ansdell, M., et al. 2018, arXiv:1803.03751
Akiyama, K., Ikeda, S., Pleau, M., et al. 2017a, AJ, 153, 159
Akiyama, K., Kuramochi, K., Ikeda, S., et al. 2017b, ApJ, 838, 1
Aleman, I., Exter, K., Ueta, T., et al. 2018, MNRAS, 477, 4499
ALMA Partnership, Brogan, C. L., Pérez, L. M., Hunter, T. R., et al. 2015, ApJL, 808, L3
Anderson, M. M., & Hallinan, G. 2017, AAS Meeting 49, 401.02
Andrews, H., Fenech, D., Prinja, R. K., Clark, J. S., & Hindson, L. 2018, MNRAS, 477, L55
Anglada, G., Rodríguez, L. F., & Carrasco-González, C. 2018, A&ARv, 26, 3
Ansdell, M., Williams, J. P., Manara, C. F., et al. 2017, AJ, 153, 240
Ayres, T. R. 2018, AJ, 156, 163
Azulay, R., Guirado, J. C., Marcaide, J. M., et al. 2015, A&A, 578, A16
Azulay, R., Guirado, J. C., Marcaide, J. M., et al. 2017a, A&A, 607, A10
Azulay, R., Guirado, J. C., Marcaide, J. M., et al. 2017b, A&A, 602, A57
Bachiller, R., Forveille, T., Huggins, P. J., & Cox, P. 1997, A&A, 324, 1123
Báez-Rubio, A., Martín-Pintado, J., Thum, C., & Planesas, P. 2013, A&A, 553, A45
Bains, I., Cohen, M., Chapman, J. M., Deacon, R. M., & Redman, M. P. 2009, MNRAS, 397, 1386
Balser, D. S., Bania, T. M., Rood, R. T., & Wilson, T. L. 1997, ApJ, 483, 320
Balser, D. S., Goss, W. M., Bania, T. M., & Rood, R. T. 2006, ApJ, 640, 360
Barrett, P. E., Dieck, C., Beasley, A. J., Singh, K. P., & Mason, P. A. 2017, AJ, 154, 252
Benaglia, P., Romero, G. E., Martí, J., Peri, C. S., & Araudo, A. T. 2010, A&A, 517, L10
Benkevitch, L. V., Sokolov, I., Oberoi, D., & Zurbuchen, T. 2010, arXiv:1006.5635
Benz, A. O., Conway, J., & Güdel, M. 1998, A&A, 331, 596
Benz, A. O., & Güdel, M. 1994, A&A, 285, 621
Booth, R. S., Vlemmings, W. H. T., & Humphreys, E. M. L. 2012, IAU Symp. S287, Cosmic Masers—from OH to H_0 (Cambridge: Cambridge Univ. Press), 31
Bower, G. C., Loinard, L., Dzib, S., et al. 2016, ApJ, 830, 107
Brookes, D. P., Stevens, I. M., Benaglia, P., Ishwara-Chandra, C. H., & Martí, J. 2016a, PhD thesis, Chapter 6 (Univ. of Birmingham)
Brookes, D. P., Stevens, I. M., & Pittard, J. M. 2016b, PhD thesis, Chapter 4 (Univ. Birmingham)
Buckley, D. A. H., Meintjes, P. J., Potter, S. B., Marsh, T. R., & Gänsicke, B. T. 2017, NatAs, 1, 29
Carrasco-González, C., Henning, T., Chandler, C. J., et al. 2016, ApJL, 821, L16
Carrasco-González, C., Rodríguez, L. F., Anglada, G., et al. 2010, Sci, 330, 1209
Castor, J. I., Abbott, D. C., & Klein, R. I. 1975, ApJ, 195, 157
Castro-Carrizo, A., Bujarrabal, V., Neri, R., et al. 2017, A&A, 600, A4
Cavallaro, F., Trigilio, C., Umana, G., et al. 2018, MNRAS, 473, 1685
Cernicharo, J., Daniel, F., Castro-Carrizo, A., et al. 2013, ApJL, 778, L25
Cernicharo, J., Gúlin, M., & Kahane, C. 2000, A&AS, 142, 181
Cerrigone, L., Umana, G., Trigilio, C., et al. 2017, MNRAS, 468, 3450
Chau, W., Zhang, Y., Nakashima, J, Deguchi, S., & Kwok, S. 2012, ApJ, 760, 66
Chen, B., Bastian, T. S., Shen, C., et al. 2015, Sci, 350, 1238
Chhetri, R., Ekers, R. D., Jones, P. A., & Ricci, R. 2013, MNRAS, 434, 956
Chomiuk, L., Linford, J. D., Yang, J., et al. 2014, Natur, 514, 339
Christensen, U. R., Holzwarth, V., & Reiners, A. 2009, Natur, 457, 167
Cohen, M., Chapman, J. M., Deacon, R. M., et al. 2006, MNRAS, 369, 189
Copley, C. J., Thondikulam, V., Loots, A., et al. 2016, arXiv:1608.02187
Coppejans, D. L., Körding, E. G., Miller-Jones, J. C. A., et al. 2015, MNRAS, 451, 3801
Coppejans, D. L., Körding, E. G., Miller-Jones, J. C. A., et al. 2016, MNRAS, 463, 2229
Coughlan, C. P., Ainsworth, R. E., Eislöffel, J., et al. 2017, ApJ, 834, 206
Crosley, M. K., & Osten, R. A. 2018, ApJ, 856, 39
Crosley, M. K., Osten, R. A., & Norman, C. 2017, ApJ, 845, 67
Cummings, J. D., Kalirai, J. S., Tremblay, P.-E., & Ramirez-Ruiz, E. 2016, ApJ, 818, 84
Daley-Yates, S., Stevens, I. R., & Crossland, T. D. 2016, MNRAS, 463, 2735
Davis, R. J., Lovell, B., Palmer, H. P., & Spencer, R. E. 1978, Natur, 273, 644
De Beck, E., & Olofsson, H. 2018, A&A, 615, 8
De Becker, M., Benaglia, P., Romero, G. E., & Peri, C. S. 2017, A&A, 600, A47
De Becker, M., & Raucq, F. 2013, A&A, 558, A28
Deguchi, S., Fujii, T., Glass, I. S., et al. 2014a, PASJ, 56, 765
Deguchi, S., Imai, H., Fujii, T., et al. 2014b, PASJ, 56, 261
de Nutte, R., Decin, L., Olofsson, H., et al. 2017, A&A, 600, A71
Dgani, R., & Soker, N. 1998, ApJL, 499, L83
Dougherty, S. M., & Taylor, A. R. 1992, Natur, 359, 808
Dressing, C. D., & Charbonneau, D. 2015, ApJ, 807, 45
Drew, P., Strelnitski, V., Smith, H. A., et al. 2017, ApJ, 851, 136
Dulaney, N. A., Richardson, N. D., Gerhartz, C. J., et al. 2017, ApJ, 836, 112
Dulk, G. A. 1985, ARA&A, 23, 169
Dupuy, T. J., Forbrich, J., Rizzuto, A., et al. 2016, ApJ, 827, 23
Duthu, A., Herpin, F., Wiesemeyer, H., et al. 2017, A&A, 604, 12

Emslie, A. G., Dennis, B. R., Shih, A. Y., et al. 2012, ApJ, 759, 71
Engle, S. G., Guinan, E. F., Harper, G. M., et al. 2017, ApJ, 838, 67
Engle, S. G., Guinan, E. F., Harper, G. M., Neilson, H. R., & Evans, N. R. 2014, ApJ, 794, 80
Evans, N. R., Pillitteri, I., Wolk, S., et al. 2016, AJ, 151, 108
Feigelson, E. D., & Montmerle, T. 1999, ARA&A, 37, 363
Fender, R., Woudt, P. A., Armstrong, R., et al. 2017, MeerKAT Science: On the Pathway to the SKA, in press (arXiv:1711.04132)
Fenech, D. M., Clark, J. S., Prinja, R. K., et al. 2018, A&A, 617, 137
Fenech, D. M., Clark, J. S., Prinja, R. K., et al. 2017, MNRAS, 464, L75
Fichtinger, B., Güdel, M., Mutel, R. L., et al. 2017, A&A, 599, A127
Finzell, T., Chomiuk, L., Metzger, B. D., et al. 2018, ApJ, 852, 108
Forbrich, J., Dupuy, T. J., Reid, M. J., et al. 2016a, ApJ, 827, 22
Forbrich, J., Osten, R. A., & Wolk, S. J. 2011, ApJ, 736, 25
Forbrich, J., Reid, M. J., Menten, K. M., et al. 2017, ApJ, 844, 109
Forbrich, J., Rivilla, V. M., Menten, K. M., et al. 2016b, ApJ, 822, 93
Forbrich, J., & Wolk, S. J. 2013, A&A, 551, A56
Freytag, B., Liljegren, S., & Höfner, S. 2017, A&A, 600, A137
Gagné, J., Faherty, J. K., Burgasser, A. J., et al. 2017, ApJL, 841, L1
Gary, D. E., Chen, B., Dennis, B. R., et al. 2018, ApJ, 863, 83
Gary, D. E., Chen, B., Nita, G. M., et al. 2017, AGU Fall Meeting, #SH41A-2755
Gary, D. E., & Hurford, G. J. 2004, in Solar and Space Weather Radiophysics, ASSL, Vol. 314, ed. D. E. Gary & C. U. Keller (Kluwer: Dordrecht), 71
Gary, D. E., White, S. M., Hurford, G. J., Nita, G. M., & Liu, Z. 2007, BAAS, 39, 216
Gérard, E., & Le Bertre, T. 2006, AJ, 132, 2566
Gérard, E., Le Bertre, T., & Libert, Y. 2011, in Proc. of the Annual Meeting of the French Society of Astronomy and Astrophysics, ed. G. Alecian et al., 419
Gillon, M., Triaud, A. H. M. J., Demory, B.-O., et al. 2017, Natur, 542, 456
Gray, M. D., Baudry, A., Richards, A. M. S., et al. 2016, MNRAS, 456, 374
Groenewegen, M. A. T., Vlemmings, W. H. T., Marigo, P., et al. 2016, A&A, 596, 50
Güdel, M. 2002, ARA&A, 40, 217
Güdel, M., & Benz, A. O. 1993, ApJ, 405, L63
Güdel, M., Benz, A. O., Schmitt, J. H. M. M., & Skinner, S. L. 1996, ApJ, 471, 1002
Guélin, M., Patel, N. A., Bremer, M., et al. 2018, A&A, 610, A4
Guinan, E. F., & Engle, S. G. 2009, in IAU Symp. 258, The Ages of Stars, ed. E. E. Mamajek, D. R. Soderbolm, & R. F. G. Wyse (Cambridge: Cambridge Univ. Press), 395
Guirado, J. C., Azulay, R., Gauza, B., et al. 2018, A&A, 610, A23
Guzman-Ramirez, L., Rizzo, J. R., Zijlstra, A. A., et al. 2016, MNRAS, 460, L35
Gvaramadze, V. V., & Menten, K. M. 2012, A&A, 541, A7
Hajduk, M., Zijlstra, A. A., van Hoof, P. A. M., et al. 2007, MNRAS, 378, 1298
Hallinan, G., & Anderson, M. M. 2017, BAAS, 49, 401.01
Hallinan, G., Antonova, A., Doyle, J. G., et al. 2006, ApJ, 653, 690
Hallinan, G., Antonova, A., Doyle, J. G., et al. 2008, ApJ, 684, 644
Hallinan, G., Bourke, S., Lane, C., et al. 2007, ApJL, 663, L25
Hallinan, G., Littlefair, S. P., Cotter, G., et al. 2015, Natur, 523, 568
Helling, C., Winters, J. M., & Sedlmayr, E. 2000, A&A, 358, 651
Hjellming, R. M. 1988, in Galactic and Extragalactic Radio Astronomy, ed. G. L. Verschuur & K. I. Kellermann (2nd ed.; New York: Springer-Verlag), 381
Hillenbrand, L. A., & White, R. J. 2004, ApJ, 604, 741
Hoai, D. T., Nhung, P. T., Gérard, E., et al. 2015, MNRAS, 449, 2386
Höfner, S., & Olofsson, H. 2018, A&ARv, 26, 1
Homan, W., Richards, A., Decin, L., et al. 2017, A&A, 601, A5
Honma, M., Akiyama, K., Uemura, M., & Ikeda, S. 2014, PASJ, 66, 95
Humphreys, E. M. L., Gray, M. D., Yates, J. A., et al. 2002, A&A, 386, 256
Humphreys, R. M., Helton, L. A., & Jones, T. J. 2007, AJ, 133, 2716
Ignace, R. 2016, MNRAS, 457, 4123
Jonas, J. 2009, IEEEP, 97, 1522
Jorgensen, U. G., & Johnson, H. R. 1992, A&A, 265, 168
Justtanont, K., Teyssier, D., Barlow, M. J., et al. 2013, A&A, 556, A101
Kamiński, T., Menten, K. M., Tylenda, R., et al. 2015, Natur, 520, 322
Kamiński, T., Menten, K. M., Tylenda, R., et al. 2017, A&A, 607, A78
Kamiński, T., Tylenda, R., Menten, K. M., et al. 2018, NatAs, 2, 778
Kao, M. M., Hallinan, G., Pineda, J. S., et al. 2016, ApJ, 818, 24
Kao, M. M., Hallinan, G., Pineda, J. S., Stevenson, D., & Burgasser, A. 2018, ApJS, 237, 25
Karmakar, S., Pandey, J. C., Airapetian, V. S., & Misra, K. 2017, ApJ, 840, 102
Katsova, M. M., & Livshits, M. A. 2015, SoPh, 290, 3663
Kerschbaum, F., Maercker, M., Brunner, M., et al. 2017, A&A, 605, A116
Kervella, P., Decin, L., Richards, A. M. S., et al. 2018, A&A, 609, A67
Kervella, P., Homan, W., Richards, A. M. S., et al. 2016, A&A, 596, 92
Klement, R., Carciofi, A. C., Rivinius, T., et al. 2017, A&A, 601, A74
Körding, E., Rupen, M., Knigge, C., et al. 2008, Sci, 320, 1318
Kozarev, K. A., Oberoi, D., Morgan, J., et al. 2016, AGU Fall Meeting, SH22B-01
Krucker, S., Giménez de Castro, C. G., Hudson, H. S., et al. 2013, A&AR, 21, 58
Kundu, M. R., Pallavicini, R., White, S. M., & Jackson, P. D. 1988, A&A, 195, 159
Lammer, H., Lichtenegger, H. I. M., Kulikov, Y. N., et al. 2007, AsBio, 7, 185
Lèbre, A., Auriére, M., Fabas, N., et al. 2014, A&A, 561, A85
Lee, U., Saio, H., & Osaki, Y. 1991, MNRAS, 250, 432
Lee, C.-F., Yang, C.-H., Sahai, R., & Sánchez Contreras, C. 2013, ApJ, 770, 153
Leto, P., Trigilio, C., Buemi, C. S., et al. 2016, MNRAS, 459, 1159
Leverenz, H., Filpović, M. D., Vukotić, B., Urošević, D., & Grieve, K. 2017, MNRAS, 468, 1794
Lim, J., Carilli, C. L., White, S. M., Beasley, A. J., & Marson, R. G. 1998, Natur, 392, 575
Linford, J. D., Chomiuk, L., Nelson, T., et al. 2017, ApJ, 842, 73
Linsky, J. L. 1996, in in ASP Conf. Ser., Vol. 93, Radio Emission from the Stars and the Sun, ed. A. R. Taylor & J. M. Paredes (San Francisco: ASP), 439
Linsky, J. L., & Haisch, B. M. 1979, ApJ, 229, L27
Lonsdale, C., Benkevitch, L., Cairns, I., et al. 2017, in Proc. of 8th International Workshop on Planetary, Solar, and Heliospheric Radio Emissions, ed. G. Fischer et al. (Vienna: Austrian Academy of Sciences Press), 425
Loukitcheva, M., White, S. M., Solanki, S. K., Fleishman, G. D., & Carlsson, M. 2017, A&A, 601, A43
Lykou, F., Klotz, D., Paladini, C., et al. 2015, A&A, 576, A46
Lynch, C. R., Lenc, E., Kaplan, D. L., Murphy, T., & Anderson, G. E. 2017, ApJL, 836, L30
Lynch, C., Mutel, R. L., & Güdel, M. 2015, ApJ, 802, 106
MacGregor, M. A., Matrà, L., Kalas, P., et al. 2017, ApJ, 842, 8
Marsh, T. R., Gänsicke, B. T., Hümmerich, S., et al. 2016, Natur, 537, 374
Matthews, L. D. 2013, PASP, 125, 313
Matthews, L. D., Le Bertre, T., Gérard, E., & Johnson, M. C. 2013, AJ, 145, 97
Matthews, L. D., Marengo, M., Evans, N. R., & Bono, G. 2012, ApJ, 744, 53
Matthews, L. D., Marengo, M., & Evans, N. R. 2016, AJ, 152, 200
Matthews, L. D., Reid, M. J., & Menten, K. M. 2015, ApJ, 808, 36
Matthews, L. D., Reid, M. J., Menten, K. M., & Akiyama, K. 2018, AJ, 156, 15
McCauley, P. I., Cairns, I. H., Morgan, J., et al. 2017, ApJ, 851, 151
McLean, M., Berger, E., Irwin, J., Forbrich, J., & Reiners, A. 2011, ApJ, 741, 27
Miller Bertolami, M. M. 2016, A&A, 588, A25
Mohan, A., & Oberoi, D. 2017, SoPh, 292, 168
Montez, R., Jr., Kastner, J. H., Balick, B., et al. 2015, ApJ, 800, 8
Mooley, K. P., Miller-Jones, J. C. A., Fender, R. P., et al. 2017, ApJL, 467, L31
Morford, J. C., Fenech, D. M., Prinja, R. K., Blomme, R., & Yates, J. A. 2016, MNRAS, 463, 763
Morford, J., Prinja, R., & Fenech, D. 2017, in IAU Symp. 316, Formation, Evolution, and Survival of Massive Star Clusters, ed. C. Charbonnel & A. Nota (Cambridge: Cambridge Univ. Press), 169
Murphy, E. J., Bolotto, A., Chatterjee, S., et al. 2018, in in ASP Conf. Ser., Monograph 7, Science with a Next-Generation Very Large Array, ed. E. J. Murphy (San Francisco, CA: ASP), in press
Mutel, R. L., Menietti, J. D., Christopher, I. W., Gurnett, D. A., & Cook, J. M. 2006, JGRA, 111, A10203

Neilson, H. R. 2014, in IAU Symp. 301, Precision Asteroseismology, ed. J. A. Guzik et al. (Cambridge: Cambridge Univ. Press), 205
Norris, R. P., Hopkins, A. M., Afonso, J., et al. 2011, PASA, 28, 215
Oberoi, D., Matthews, L. D., Cairns, I. H., et al. 2011, ApJL, 728, L27
O'Gorman, E., Harper, G. M., Brown, A., et al. 2015, A&A, 580, A101
O'Gorman, E., Kervella, P., Harper, G. M., et al. 2017, A&A, 602, L10
Ortiz-Léon, G. N., Loinard, L., Kounkel, M. A., et al. 2017, ApJ, 834, 141
Osten, R. A., & Crosley, M. K. 2017, Next Generation Very Large Array Memo, 31, http://library.nrao.edu/public/memos/ngvla/NGVLA_31.pdf
Osten, R. A., Kowalski, A., Drake, S. A., et al. 2016, ApJ, 832, 174
Osten, R. A., & Wolk, S. J. 2015, ApJ, 809, 79
Padovani, M., Hennebelle, P., Marcowith, A., & Ferrière, K. 2015, A&A, 582, L13
Pandya, A., Zhang, Z., Chandra, M., & Gammie, C. F. 2016, ApJ, 822, 34
Pardo, J. R., Cernicharo, J., Gonzalez-Alfonso, E., & Bujarrabal, V. 1998, A&A, 329, 219
Paredes, J. M. 2005, EAS, 15, 187
Patel, N. A., Gottlieb, C., Young, K., et al. 2018, AAS Meeting 231, 408.06
Patel, N., Young, K. H., Gottlieb, C. A., et al. 2011, ApJS, 193, 17
Pérez-Sánchez, A. F., Tafoya, D., García López, R., Vlemmings, W., & Rodríguez, L. F. 2017, A&A, 601, A68
Pérez-Sánchez, A. F., Vlemmings, W. H. T., Tafoya, D., & Chapman, J. M. 2013, MNRAS, 436, L79
Pineda, J. S., & Hallinan, G. 2018, ApJ, 866, 155
Pineda, J. S., Hallinan, G., & Kao, M. M. 2017, ApJ, 846, 75
Pottasch, S. R., & Bernard-Salas, J. 2013, A&A, 550, A35
Primiani, R. A., Young, K. H., Young, A., et al. 2016, JAI, 5, 1641006
Quiroga-Nũnez, L. H., van Langenvelde, H. J., Pihlström, Y. M., Sjouwerman, L. O., & Brown, A. G. A. 2018, in IAU Symp. 330, Astronomy and Astrophysics in the Gaia Sky, ed. A. Recio-Blanco (Cambridge: Cambridge Univ. Press), 245
Ramstedt, S., & Olofsson, H. 2014, A&A, 566, A145
Raulin, J.-P., Lüthi, T., Trottet, G., & Correia, E. 2004, COSPAR, 35, 3118
Reid, M., Loinard, L., & Maccarone, T. 2018, in ASP Conf. Series, Monograph 7, Science with a Next-Generation Very Large Array, ed. E. J. Murphy (San Francisco, CA: ASP) in press
Reid, M. J., & Menten, K. M. 1997, ApJ, 476, 327
Reid, M. J., Menten, K. M., Brunthaler, A., et al. 2014, ApJ, 783, 130
Richards, A. M. S., Davis, R. J., Decin, L., et al. 2013, MNRAS, 432, L61
Richards, A. M. S., Gray, M. D., Baudry, A., et al. E.M.L. 2018, in IAU Symp. 336, Astrophysical Masers: Unlocking the Mysteries of the Universe, ed. A. Tarchi, M. J. Reid, & P. Castangia (Cambridge: Cambridge Univ. Press), 347
Richards, A. M. S., Impellizzeri, C. M. V., Humphreys, E. M., et al. 2014, A&A, 572, L9
Riggi, S., Ingallinera, A., Leto, P., et al. 2016, MNRAS, 460, 1468
Rodríguez-Kamenetzky, A., Carrasco-González, C., Araudo, A., et al. 2016, ApJ, 818, 27
Route, M. 2017, ApJ, 845, 66
Route, M., & Wolszczan, A. 2012, ApJL, 747, L22
Rowlinson, A., Bell, M. E., Murphy, T., et al. 2016, MNRAS, 458, 3506
Ruffle, P. M. E., Zijlstra, A. A., Walsh, J. R., et al. 2004, MNRAS, 353, 796
Safarzadeh, M., Lu, Y., & Hayward, C. C. 2017, MNRAS, 472, 2462
Sahai, R., Vlemmings, W. H. T., & Nyman, L. Å. 2017, ApJ, 841, 110
Sánchez-Contreras, C., Báez-Rubio, A., Alcolea, J., Bujarrabal, V., & Martín-Pintado, J. 2017, A&A, 603, A67
Sanna, A., Reid, M. J., Dame, T. M., Menten, K. M., & Brunthaler, A. 2017, Sci, 358, 227
Santander-García, M., Bujarrabal, V., Alcolea, J., et al. 2017, A&A, 597, A27
Segura, A., Walkowicz, L. M., Meadows, V., Kasting, J., & Hawley, S. 2010, AsBio, 10, 751
Semel, M. 1989, A&A, 225, 456
Shara, M. M., Moffat, A. F. J., & Webbink, R. F. 1985, ApJ, 294, 271
Sharma, R., Oberoi, D., & Arjunwadkar, M. 2018, ApJ, 852, 69
Shmeld, I. K., Strelnitskij, V. S., Fedorova, A. V., & Fedorova, O. V. 1992, in IAU Symp. 150, Astrochemistry of Cosmic Phenomena, ed. P. D. Singh (Dordrecht: Kluwer Academic Publishers), 413
Shibayama, T., Maehara, H., Natsu, S., et al. 2013, ApJS, 209, 5
Sjouwerman, L. O., Capen, S. M., & Claussen, M. J. 2009, ApJ, 705, 1554
Smith, K., Güdel, M., & Audard, M. 2005, A&A, 436, 241
Soker, N., & Lasota, J.-P. 2004, A&A, 422, 1039
Spangler, S. R., & Moffett, T. J. 1976, ApJ, 203, 497
Strelnitski, V., Bieging, J. H., Hora, J., et al. 2013, ApJ, 777, 89
Stroh, M. C., Pihlström, Y. M., Sjouwerman, L. O., et al. 2018, ApJ, 862, 153
Suresh, A., Sharma, R., Oberoi, D., et al. 2017, ApJ, 843, 19
Suzuki, T. K. 2007, ApJ, 59, 1592
te Lintel Hekkert, P., Dejonghe, H., & Habing, H. J. 1991, PASAu, 9, 20
Thomashow, E., Jorgenson, R. A., Strelnitski, V., Walter, G. & Maria Mitchell Observatory Research Experience for Undergraduates Interns 2018, AAS Meeting 231, 136.10
Tingay, S. J., Hancock, P. J., Wayth, R. B., et al. 2016, AJ, 152, 82
Trapp, A. C., Rich, R. M., Morris, M. R., et al. 2018, ApJ, 861, 75
Treumann, R. A. 2006, A&ARv, 13, 229
Trigilio, C., Umana, G., Buemi, C. S., & Leone, F. 2011, ApJL, 739, L10
Trigilio, C., Umana, G., Cavallaro, F., et al. 2018, MNRAS, 481, 217
Tsuji, T. 2000, ApJ, 540, L99
Tsuji, T. 2001, in IAU Symp. 205, Galaxies and their Constituents at the Highest Angular Resolutions, ed. R. T. Schilizzi (Singapore: World Scientific), 316
Tylenda, R., Kamiński, T., Udalski, A., et al. 2013, A&A, 555, A16
Umana, G., Trigilio, C., & Cerrigone, L. 2015a, in Proc., of Advancing Astrophysics with the Square Kilometre Array (Giardini Naxos, Italy), 118
Umana, G., Trigilio, C., Franzen, T. M. O., et al. 2015b, MNRAS, 454, 902
Van de Sande, M., Decin, L., Lombaert, R., et al. 2018, A&A, 609, A63
Vassiliadis, E., & Wood, P. R. 1993, ApJ, 413, 641
Velilla Prieto, L., Sánchez Contreras, C., Cernicharo, J., et al. 2017, A&A, 597, A25
Villadsen, J., Hallinan, G., Bourke, S., Güdel, M., & Rupen, M. 2014, ApJ, 788, 112
Villadsen, J., Hallinan, G., Bourke, S., & Monroe, R. 2017, BAAS, 49, 400.04
Vlemmings, W., Khouri, T., O'Gorman, E., et al. 2017, NatAs, 1, 848
Waters, L. B. F. M., van der Veen, W. E. C. J., Taylor, A. R., Marlborough, J. M., & Dougherty, S. M. 1991, A&A, 244, 120
Wedemeyer, S., Bastian, T., Brajša, R., et al. 2016, SSRv, 200, 1
Welch, D. L., & Duric, N. 1988, AJ, 95, 1794
Wendeln, C., Chomiuk, L., Finzell, T., Linford, J. D., & Strader, J. 2017, ApJ, 840, 110
Weston, J. H. S., Sokoloski, J. L., Chomiuk, L., et al. 2016a, MNRAS, 460, 2687
Weston, J. H. S., Sokoloski, J. L., Metzger, B. D., et al. 2016b, MNRAS, 457, 887
White, R. L. 1985, ApJ, 289, 698
White, S. M. 2004, in Solar and Space Weather Radiophysics, ed. D. E. Gary & C. U. Keller (Dordrecht: Kluwer), 89
White, S. M. 2007, AsJPh, 16, 189
White, S. M., & Franciosini, E. 1995, ApJ, 444, 342
White, S. M., Iwai, K., & Phillips, N. M. 2017, SoPh, 292, 88
Williams, P. K. G. 2017, Handbook of Exoplanets, submitted (arXiv:1707.04264)
Williams, P. K. G., Casewell, S. L., Stark, C. R., et al. 2015, ApJ, 815, 64
Winters, J. G., Henry, T. J., Lurie, J. C., et al. 2015, AJ, 149, 5
Withers, P., & Vogt, M. F. 2017, ApJ, 836, 114
Wolk, S. J., Pillitteri, I., & Poppenhaeger, K. 2017, in IAU Symp. 328, Living Around Active Stars (Cambridge: Cambridge Univ. Press), 290
Wright, A. E., & Barlow, M. J. 1975, MNRAS, 170, 41
Yusef-Zadeh, F., Bushouse, H., Schödel, R., et al. 2015a, ApJ, 809, 10
Yusef-Zadeh, F., Cotton, B., Wardle, M., et al. 2017a, MNRAS, 467, 922
Yusef-Zadeh, F., Roberts, D. A., Wardle, M., et al. 2015b, ApJL, 801, L26
Yusef-Zadeh, F., Wardle, M., Cotton, W., et al. 2017b, ApJ, 837, 93
Yusef-Zadeh, F., Wardle, M., Kunneriath, D., et al. 2017c, ApJL, 850, L30
Zhang, Q., Claus, B., Watson, L., & Moran, J. 2017, ApJ, 837, 53
Zhang, Y., Kwok, S., & Dihn-V-Trung 2009, ApJ, 691, 1660
Zijlstra, A. A., Pottasch, S. R., & Bignell, C. 1989, A&AS, 79, 329
Zijlstra, A. A., van Hoof, P. A. M., & Perley, R. A. 2008, ApJ, 681, 1296